PAGE-ICE IAM, v6.22

Technical Description

Dmitry Yumashev

Lancaster, April 2019

Table of Contents

Glossary

AF	Amplification factor
BAU	Business as usual
CMIP5	Climate models inter-comparison project, phase 5
CMIP3	Climate models inter-comparison project, phase 3
DICE	Dynamic integrated climate-economy (IAM)
ECS	Equilibrium climate sensitivity
FRT	Feedback response time
FUND	Framework for uncertainty, negotiation and distribution (IAM)
GCM	General circulation model (coupled atmosphere, ocean and land)
GHG	Greenhouse gas
GMST	Global mean surface temperature
GWP	Global warming potential
IAM	Integrated assessment model
NDCs	Nationally determined contributions
JULES	Joint UK Land Environment Simulator
LSM	Land surface model
PAGE	Policy analysis of greenhouse effect (IAM)
PAGE-ICE	PAGE – ice, climate and economics
PCF	Permafrost carbon feedback
RCP	Representative concentration pathway
RF	Radiative forcing
SAF	Surface albedo feedback
SiBCASA	Simple Biosphere/Carnegie-Ames-Stanford Approach
SLR	Sea level rise
SPM	Summary for policy-makers
SRES	Special report on emissions scenarios
SSP	Shared socio-economic pathway
TCR	Transient climate response

PAGE-ICE v6.22: basic description and system requirements

Authorship, acronyms and key functionalities

PAGE-ICE Nonlinear Arctic Feedbacks   Version   6.22   Date   20/03/2019

Lead author	Dmitry Yumashev	Lancaster University
Contributing author	Chris Hope	University of Cambridge
Original developer of the PAGE model	Chris Hope	University of Cambridge

PAGE = Policy Analysis of Greenhouse Effect
ICE = Ice, Climate, Economics

Nonlinear Arctic Feedbacks: PCF = permafrost carbon feedback; SAF = surface albedo feedback driven by loss of the sea ice and land snow covers

PAGE-ICE is the latest version of the PAGE model as of March 2019. Previous versions: PAGE09, PAGE2002. These three versions are implemented in Excel and utilise symbolic notations along with array formulae extensively.

An open source Julia version of PAGE-ICE will be made available on the Mimi platform shortly. For further details see https://www.mimiframework.org/

PAGE-ICE simulates World A, World B and World A-B, allowing one to perform the following statistical experiments across a wide range of climate and socio-economic scenarios:

- Experiment Family 1: Sensitivity of global climate and economy to nonlinear Arctic feedbacks (PCF and SAF) under a given scenario
- Experiment Family 2: SCCO2 either with the nonlinear or legacy Arctic feedbacks (PCF = 0, SAF = const in line with the 2xCO2 ECS parameter)
- Experiment Family 3: Comparison between two scenarios, either with the nonlinear or legacy Arctic feedbacks

System requirements

- Microsoft Windows 7 or higher
- Microsoft Excel 2013 or higher
- @RISK 6.x or higher. Add-in by Palisade allowing one to run statistical (Monte-Carlo) simulations in Excel. Free trial version of @RISK is available at https://www.palisade.com/trials.asp

Description of the individual sheets in the PAGE-ICE workbook

Cockpit	Use the drop down menus to choose the experiment, the underlying climate and socio-economic scenarios, the economic impact function, the weighting and discounting
Results	Statistical post-processing of the key results for the Worlds A, B and A-B
Base data	Climate and socio-economic data for the base year 2015 required to initiate the model, along with the key model settings and the repository of the RCP and SSP scenarios
Library data	Climate and socio-economic parameters of the model with uncertainty. The uncertainty ranges are calibrated according to the latest literature when the data is available, and are expert judgements otherwise. The default probability distributions are subjective in most cases
Policy A, B, and A-B	Chosen mitigation pathways and planned adaptation policies for the Worlds A, B and A-B
Emissions A, B and A-B	Emissions corresponding to the chosen mitigation pathways

Climate A, B and A-B	Future climates in the Worlds A, B and A-B driven by the given emissions pathways and the chosen representations of the Arctic feedbacks (either nonlinear or legacy)
Economy A, B and A-B	Future GDP and population (POP) under the chosen socio-economic pathways, along with the corresponding equity weights and discounting factors
Preventative costs A, B and A-B	Mitigation costs corresponding to the chosen mitigation pathways
Adaptive costs A, B and A-B	Adaptation costs corresponding to the chosen adaptation policy
Impacts A, B and A-B	Impacts due to climate change under the chosen mitigation and adaptation policies. The following impacts categories are included: sea level rise, economic, non-economic, discontinuity
Totals	Summary of the mitigation costs, adaptation costs and climate-driven impacts, and the total economic effect of climate change, for the Worlds A, B and A-B

Introduction

PAGE-ICE (v6.22) is based on the PAGE09 IAM (Hope, 2006; Hope, 2013). It includes several updates both to climate science and economics from IPCC AR5 and literature that followed, as well as several novel developments presented in the study "*Climate policy implications of nonlinear decline of Arctic land permafrost and other cryosphere elements*" (Yumashev et al., 2019). The majority of the work was funded by the European Commission (ICE-ARC project, grant 603887).

Generic updates in PAGE-ICE: (i) adjusted analysis years starting with 2015 (base year), 2020, 2030, 2040, 2050, 2075, 2100, 2150, 2200, 2250 and 2300, allowing for a better representation of the essential long-term processes: permafrost emissions, winter sea ice and land snow decline and melting of the ice sheets; (ii) updated base year (2015) data for the emissions, temperature, population, GDP-PPP, cumulative permafrost emissions and surface albedo feedback, with uncertainty ranges for most parameters; (iii) updated set of emissions (RCP) and socio-economic (SSP) scenarios paired according to the RCP-SSP compatibility conditions (Riahi et al., 2017) and modified to cover the range of scenarios in line with the Paris Agreement, as well as the possibility of a reversal of climate policies in the US and globally.

Climate science updates in PAGE-ICE: (i) internal dynamic representation of the nonlinear PCF and SAF using emulators based on simulations from multiple CMIP5 and CMIP3 GCMs and SiBCASA and JULES LSMs run under the extended RCP8.5, 4.5 and 2.6 (only JULES) scenarios out to 2300; (ii) adjusted transient climate response (TCR), feedback response time (FRT) and ECS parameter ranges according to IPCC AR5 based on CMIP5 models, paleo-records and climate models of intermediate complexity; (iii) revised CO_2 cycle in line with the latest multi-model assessment of the atmospheric CO_2 response function (Joos et al., 2013); (iv) improved

GMST equation using a better numerical scheme for finite analysis periods; (v) CMIP5-based amplification factors for the regional temperatures; (vi) changes in the implementation of the regional sulphate cooling: sulphates now add to the global forcing and affect the regional temperatures implicitly through the CMIP5-based amplification factors (their RF is not included in the regional temperature equation directly due to the complexity of climatic response to regional RFs, which requires regional climate sensitivities to be introduced; Shindell & Faluvegi, 2009); (vii) approximately halved indirect sulphate cooling effect; (viii) fat-tailed distribution for the sea level rise (SLR) time lag (at the lower values end) to account for the possible acceleration in the discharge from the West Antarctica and Greenland ice sheets (Golledge et al., 2015; Hansen et al., 2016; Le Bars et al., 2017; Nauels et al., 2017).

Economics updates in PAGE-ICE: (i) new economic impact function based on the recent macro-econometric analysis of the effect of historic temperature shocks on economic growth in multiple countries by Burke et al. (2015) projected onto the 8 major regions of the PAGE model using population-weighted temperatures, and adapted to fit with the single year consumption-only approach for climate impacts used in PAGE; (ii) considerably downscaled saturation limit for the impacts; (iii) modified uncertainty range for the "business as usual" emissions scenario, which is used as a reference point for calculating the abatement costs, covering the range roughly between RCP6.0 and a pathway exceeding RCP8.5 (Christensen et al., 2018); (iv) revised present-day marginal abatement cost (MAC) curves (Aldy et al., 2016), technological learning rate (CO_2 only) (Rubin et al., 2015) and autonomous technological change based on energy efficiency improvements (IEA, 2012); (v) significantly downscaled discontinuity sector, which now accounts only for socio-economic tipping points such as pandemics, mass migration and wars, as well as possible other tipping points in the climate than permafrost, sea ice, land snow and lea level rise from ice sheets (the catastrophic loss of the ice sheets has been moved to the fat-tailed distribution in the sea level rise module); (vi) reduced tolerable temperature rise that gives no chance of a discontinuity; (vi) significantly decreased time constant of a discontinuity in line with its new interpretation; (vii) focus on autonomous adaptation as part of the Burke et al. economic impact function, with planned adaptation restricted to SLR impacts.

Overview of the PAGE model

The PAGE IAM (Hope, 2006; Hope, 2013) splits the world into 8 large geopolitical regions: EU, US, other OECD countries (OT), former Soviet Union (EE), China+ (CA), India+ (IA), Africa and Middle East (AF) and Latin America (LA). It estimates climate-driven impacts in each region across four broad categories: sea level rise (coastal flood damage, relocation), economic (both direct and indirect damages to the aggregate economy), non-economic (ecosystems services, public health) and discontinuity (large-scale damages associated with a number of possible tipping points in the climate and economy).[1] Anthropogenic GHG emissions are split into 6 main classes: CO_2, CH_4, N_2O, linear gases (PFCs, HFC and SF6, sometimes referred to as High GWP gases), sulphate aerosols and the rest of GHGs combined (tropospheric O_3, BC aerosols,

---

[1] PAGE-ICE re-defines the discontinuity impacts sector as being related primarily to the possible large-scale socio-economic effects of climate change such as mass migrations, pandemics and wars, as well as all the other climatic tipping points apart from land permafrost, Arctic sea ice and the two ice sheets.

OC aerosols, CFCs and HCFCs), and follow IPCC scenarios (SRES or RCPs) extended until year 2200 (2300 in PAGE-ICE). A simple aggregate climate model is used to link the emissions with global temperature rise, which is then scaled for each of the 8 regions and is also used to drive sea level rise as well as the discontinuity impacts.

The rise in regional temperatures serves as a basis for evaluating economic and non-economic impacts, which are calculated as percentage loss/gain of the relevant regional/global GDP in a given future year, and are subtracted from consumption only; endogenous effects on economic growth are not considered in the default model setting. Future GDP and population projections in the 8 world regions follow exogenous scenarios from IPCC (SRES or SSPs). The impacts depend on the increases in the regional temperatures and sea level relative to the corresponding tolerable levels determined by the choice of adaptation spending in each of the 8 regions. The total economic effect of climate change, therefore, consists of mitigation costs (which depend on the levels of ambition in each region under a given emissions scenario), adaptation costs and residual climate impacts. Calculated separately in each region, the total economic effects are equity-weighted depending on the region's relative wealth (Anthoff et al., 2009), and are discounted to the base year (2015 in the default PAGE-ICE setting) using a pure time preference rate and aggregated.

The multiple uncertainties in the global climate and economy are accounted for by performing Monte-Carlo simulations, with over 150 uncertain inputs such as climate sensitivity to CO_2, convexity of the damage functions and discount rates are calibrated using expert climate and economic models (see Table 12). Due to the limitations of the data, especially when it comes to estimating the impacts of climate change on the economy, most of the input probability distributions are subjective and are approximated by triangular distributions. All the outputs are also in the form of probability distributions.

Discounting

We do not just aggregate the economic impacts over each analysis period in PAGE-ICE, but also discount them in line with a standard methodology adopted from finance, which is common in climate policy assessments based on cost-benefit analysis. The main indicator employed in the analysis is the Net Present Value (NPV) of the economic effect of climate change and, specifically, of the Arctic feedbacks. It uses the discounting with a pure time preference rate, along with equity weighting based on changes in the marginal utility of consumption with income (Anthoff et al., 2009). As a result, the further in future the impacts are, the less they contribute to the NPV calculation, making the result very different from a simple aggregation. Despite the reduced weight, the impacts that are set to occur in the 22nd and 23rd centuries, i.e. on the timescales associated with the relatively slow climate feedbacks such as carbon emissions from thawing permafrost and sea level rise from melting ice sheets, make an essential contribution to NPV of the total economic effect of climate change.

Statistical simulations vs inter-annual variability

PAGE and similar IAMs do not model natural climate variability, and therefore each Monte-Carlo run is deterministic in time. This allows one to work with Monte-Carlo generated probability distributions of multiple climatic and economic parameters in any fixed analysis year like 2100, as opposed to taking averages over the 30-year climatological windows (a standard requirement for any climate model data with multiple natural variability cycles).

Climate scenarios and model setup in PAGE-ICE

We defined the scenarios consistent with the Paris Agreement and current climate change projections by pairing representative concentration pathways (RCPs) and shared socio-economic pathways (SSPs) according to the feasible ranges of emissions for each of the five main SSPs (Riahi et al., 2017; Christensen et al., 2018). Table 1 summarises the scenarios. The imaginary "Zero Emissions" scenario in which all global emissions stop in the base year 2020 characterises the effect of the historic emissions on the PCF and SAF.

Table 1. Climate and socio-economic scenarios obtained by pairing RCPs with SSPs. Source: Yumashev et al. (2019).

Scenario	Description
Zero Emissions	GHG emissions stop immediately after 2020
1.5°C Target	50% chance of staying below 1.5°C relative to pre-industrial in 2100
2°C Target	50% chance of staying below 2°C relative to pre-industrial in 2100
2.5°C Target	50% chance of staying below 2.5°C relative to pre-industrial in 2100
NDCs	Current nationally determined contributions (pledges) to reducing GHG emissions
NDCs Partial	Around 30% of the NDCs are not met, consistent with long-term effects of the US's withdrawal
Business as usual (BaU)	Projections for GHG emissions without NDCs

First, we defined the "medium" SSPM scenario by averaging SSP2, SSP3 and SSP4 with equal weights, and paired it with RCP4.5 to represent a likely world with medium levels of emissions. Second, we paired SSP1 with RCP2.6 and SSP5 with RCP8.5, which represents the likely lower and the upper ends of the emissions range and the associated socio-economic makeup of the world. Using these low, medium and high emissions pairs, we introduced a weighting scheme that covers the entire range as the weighting parameter w changes from -1 (lower end) to $+1$ (upper end):

$$\begin{Bmatrix} \text{SSPW} \\ \text{RCPW} \end{Bmatrix} = \left(\frac{1-w}{2}\right)^2 \cdot \begin{Bmatrix} \text{SSP1} \\ \text{RCP2.6} \end{Bmatrix} + \frac{1-w^2}{2} \cdot \begin{Bmatrix} \text{SSPM} \\ \text{RCP4.5} \end{Bmatrix} + \left(\frac{1+w}{2}\right)^2 \cdot \begin{Bmatrix} \text{SSP5} \\ \text{RCP8.5} \end{Bmatrix}$$

A statistical optimisation algorithm (Risk Optimiser) was then employed in PAGE-ICE to find the values of w that result in a 50% chance for the GMST in 2100 to reach the levels consistent

with: (i) NDCs from the Paris Agreement extrapolated until 2100 (3.3°C, $w = -0.14$),[2] (ii) partially implemented NDCs representing an estimated long-term effect of the US's withdrawal from the NDCs (3.6°C, $w = 0.1$),[3] and (iii) business as usual projections without the Paris Agreement (4.2°C, $w = 0.52$).[4] We also added a 2.5°C target scenario ($w = -0.7$) which is more ambitious than the NDCs but falls short of the 2°C target.

The 1.5°C and 2°C scenarios, defined as having a 50% chance of keeping the GMST rise in 2100 below the 1.5°C and 2°C targets based on PAGE-ICE simulations, require extra abatement relative to RCP2.6. They fall outside the range covered by the SSPW and RCPW pairs described above. We therefore introduced an additional abatement rate relative to RCP2.6, the same for all the major GHGs represented in PAGE-ICE, and employed Risk Optimiser to find that it is equal to 0.24% per year for the 2°C target and 4.05% per year for the 2°C target scenario. Both of these scenarios overshoot their respective targets during the second half of the 21st century and imply negative CO_2 emissions thereafter.

Figure 1 shows the medians and 25-75% ranges for the GMST projections relative to pre-industrial levels for the climate scenarios considered, obtained using PAGE-ICE with the legacy values of the PCF and SAF (see the caption).
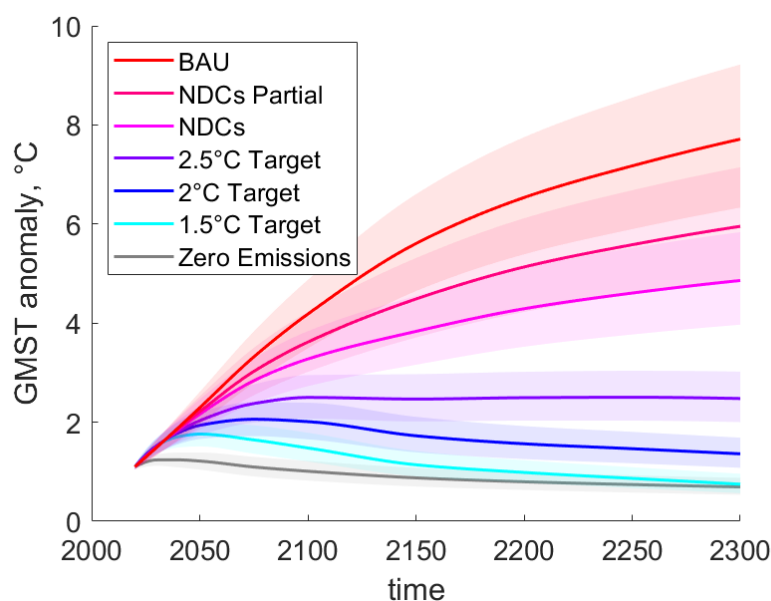
Figure 1. Median GMST projections relative to pre-industrial 1850-1900 levels (thick lines) and the relevant 25-75% ranges (shaded areas) obtained from 100,000 runs of PAGE-ICE for all the climate scenarios considered, assuming the following legacy values of the PCF and SAF: zero permafrost emissions, constant SAF of 0.35±0.05 W m^{-2} K^{-1} (corresponding to 2xCO2 ECS parameter). This serves as a base estimate for the subsequent analysis of the nonlinear PCF and SAF. Source: Yumashev et al. (2019).

---

[2] https://www.climateinteractive.org, accessed on 09 September 2017.
[3] https://www.climateinteractive.org/analysis/us-role-in-paris/, accessed on 09 September 2017.
[4] https://www.climateinteractive.org, accessed on 09 September 2017.

Implementation of the RCP and SSP scenarios and their modifications

RCP scenarios

The RCP database[5] provides emissions in 5 world regions, while PAGE IAM has 8 regions (see above). For CO_2, CH_4, N_2O and sulphates, we use the following mapping of the RCP regions onto the PAGE regions:

- R5ASIA to CA and IA
- R5LAM to LA
- R5MAF to AF
- R5OECD to EU, US and OT
- R5REF to EE

For the linear gases, we used modifications of the SRES A1B scenario to approximate the linear gases emissions for RCP4.5 and RCP8.5, and assumed that the Kigali Agreement on phasing out HFCs[6] applies to all regions under RCP2.6.

For the excess forcing, we used modifications of the SRES A1B scenario for tropospheric O_3, BC Aerosols, OC aerosols, CFCs and HCFCs to approximate the excess RF for RCP4.5 and RCP8.5, and adopted the 2016r5low scenario developed by the UK Met Office to provide the excess RF projections for RCP2.6.

The emissions projections for the RCP scenarios are available until 2100. To run PAGE-ICE out to 2300, we assume constant rates of emissions beyond 2100 for all GHGs, which is consistent with the approach used in the selected CMIP5 runs that were extended out to 2300. All the RCP scenarios in PAGE-ICE are emissions-driven,[7] unlike the concentration-driven RCP scenarios that were used in most CMIP5 experiments (Taylor et al., 2012).

The RCP2.6 scenario is based on aggressive early mitigation combined with extensive carbon capture and storage activities, which effectively implies negative net emissions in the latter parts of the 21st century (Van Vuuren et al., 2011).

RCP2.6e scenario

The RCP2.6e scenario follows RCP2.6 with an additional abatement that gives a 50% chance of keeping the GMST increase below either the 1.5°C target or the 2°C target in 2100. The extra abatement is implemented as a ratcheting-up cutback to annual RCP2.6 emissions (same for each of the 6 "policy gases" implemented in PAGE, see above) governed by a compound annual abatement rate, starting in 2020 and running until 2100, which is determined using Risk Optimiser separately for either of the two GMST targets. The marginal abatement cost

---

[5] https://tntcat.iiasa.ac.at/RcpDb/dsd?Action=htmlpage&page=welcome

[6] http://www.unep.org/africa/news/kigali-amendment-montreal-protocol-another-global-commitment-stop-climate-change

[7] https://tntcat.iiasa.ac.at/RcpDb/dsd?Action=htmlpage&page=welcome, accessed on 30 September 2017.

curve in PAGE-ICE allows one to quantify the very high abatement costs associated both with RCP2.6 and RCP2.6e.

For a given RCP scenario such as RCP2.6, the reductions and/or increases of annual emissions of a selected GHG relative to their base year level E_0 (Mton/yr) can be described by the equation

$$E_t = E_0 \cdot \prod_{t_i=t_0}^{t_i=t} \left(1 - r_{t_i}\right)$$

where t_0 is the base year, E_t is the projected level of annual emissions in a future year t before 2100, and r_{t_i} are the annual rates of change in future years $t_i \in [t_0, t]$. According to this definition, negative rates r_{t_i} imply emissions increases in a given year.

Introducing a constant extra rate of abatement r_e (per annum) transforms the formula to

$$E_{t,extra} = E_0 \cdot (1 - r_e)^{t-t_0} \cdot \prod_{t_i=t_0}^{t_i=t} \left(1 + r_{t_i}\right)$$

This formula is implemented for all the "policy gases" in PAGE-ICE (with unique rates for each gas according to the relevant RCP projections) apart from CO_2. CO_2 is the only GHG which reaches negative emissions in the latter parts of the 21st century under the RCP2.6 scenario. The corresponding negative emissions level in 2100 from RCP2.6, denoted as $E_{2100}^{(CO_2)} < 0$, is used to put a constraint on the long-term CO_2 cutback under the RCP2.6e scenario:

$$E_{t,extra}^{(CO_2)} = E_{2100}^{(CO_2)} + \left(E_0^{(CO_2)} - E_{2100}^{(CO_2)}\right) \cdot \left(1 - r_e^{(CO_2)}\right)^{t-t_0} \cdot \prod_{t_i=t_0}^{t_i=t} \left(1 + r_{t_i}^{(CO_2)}\right)$$

These formulae are applicable for t running until 2100. Beyond 2100, annual emission rates for all the GHGs are assumed to be constant:

$$E_t = E_{2100}, \quad t > 2100$$

SSP scenarios

PAGE-ICE uses annual rates of GDP and population change, denoted as $\dot{Y}$ and $\dot{P}$, which are taken from the SSP database[8] and mapped on the 8 PAGE regions. We consider all five SSP scenarios and match them with the relevant RCP scenarios for the emissions according to the RCP-SSP compatibility conditions (Riahi et al., 2017). The more socio-economically unstable and risky SSP3 "regional rivalry" and SSP4 "inequality" scenarios are combined with "middle of the road" SSP2 to define the "medium" SSPM pathway, which is then paired with the medium RCP4.5 emissions scenario. Along with the extreme end pairs SSP1 & RCP2.6 and SSP5 & RCP8.5, the SSPM & RCP4.5 pair provides a plausible development pathway for a word with medium levels of emissions.

---

[8] https://tntcat.iiasa.ac.at/SspDb/dsd?Action=htmlpage&page=about

The SSP scenarios run until 2100. To extend $\dot{Y}$ out to 2300 while maintaining the trends predicted by the SSP scenarios in the latter parts of the 21st century, we use an exponential extrapolation based on the SSP values in the two final analysis years of the PAGE model that fall within the 21st century: 2075 and 2100. The assumption is that if $\dot{Y}$ is positive in 2100, it subsequently tends to zero exponentially on the long run, while negative $\dot{Y}$ in 2100 is kept constant until 2300. The extrapolation for $t > 2100$ is therefore defined as

$$\dot{Y}_t = \begin{cases} \dot{Y}_{2100} \cdot \exp\left(\dfrac{t - 2100}{\tau_Y}\right), & \tau_Y = (2100 - 2075) \cdot \left[\ln\left(\dfrac{\dot{Y}_{2075}}{\dot{Y}_{2100}}\right)\right]^{-1}, \quad \dot{Y}_{2100} > 0 \\[2em] \dot{Y}_{2100}, \quad \dot{Y}_{2100} < 0 \end{cases}$$

The population growth rates $\dot{P}$, on the other hand, are kept equal to zero beyond 2100 for all the SSP scenarios used.

CO₂ cycle from Joos et al. (2013)

We base the new CO_2 cycle in PAGE-ICE on the latest multi-model assessment of the atmospheric CO_2 response function by Joos et al. (2013). The models used include several CMIP5 GCMs, as well as a number of climate and carbon cycle models of intermediate complexity. All the models were run with the initial pulse of 100 GtC for up to up to $\tau_{max} = 1000$ years. The resulting response function is applicable only on these timescales and has four components:

$$f(\tau) = a_0 + \sum_{n=1}^{3} a_n \cdot \exp\left(-\frac{\tau}{\tau_n}\right), \quad a_0 = 1 - \sum_{n=1}^{3} a_n$$

Equation 1

Neither of the components has direct physical meaning, although they could be associated broadly with long-term ocean uptake (a_1, τ_1), short-term ocean uptake (a_2, τ_2) and land uptake (a_3, τ_3) processes. The a_0 terms represents the CO_2 asymptote applicable on the timescales of a millennium (too short for rock weathering to occur). Together, the components of the response function in Equation 1 represent one of the best possible empirical fits to the simulations results from each model in the chosen ensemble.

Each model m is characterised its own set of coefficients $\{a_n, \tau_n\}_m$, which are provided in the supplementary materials by Joos et al. We used these coefficients to reconstruct a unique response function $f_m(\tau)$ for each model. The multi-model mean and SD of these functions, denoted as $\mu(f_m(\tau))$ and $\sigma(f_m(\tau))$, are plotted in Figure 2. Introducing a new function $f(\tau)$ using Equation 1, with specified uncertainty ranges for all the parameters $\{a_n, \tau_n\}$, we simulated this function multiple times to obtain the corresponding Monte-Carlo mean and SD, denoted as $M(f(\tau))$ and $S(f(\tau))$. Assuming triangular distributions for $\{a_n, \tau_n\}$, we then ran a statistical optimisation algorithm provided by @Risk Optimiser to find the optimal uncertainty ranges for these distributions that minimise the root mean square misfits

simultaneously for the Monte-Carlo mean and SD of the response function relative to the corresponding multi-model mean and SD:

$$\varepsilon_M = \left[\frac{1}{\tau_{max}} \cdot \int_0^{\tau_{max}} \Big(M(f(\tau)) - \mu(f_m(\tau)) \Big)^2 \, d\tau \right]^{\frac{1}{2}}$$

$$\varepsilon_S = \left[\frac{1}{\tau_{max}} \cdot \int_0^{\tau_{max}} \Big(S(f(\tau)) - \sigma(f_m(\tau)) \Big)^2 \, d\tau \right]^{\frac{1}{2}}$$

The resulting optimal $M(f(\tau))$ and $S(f(\tau))$ are plotted in Figure 2, and the associated uncertainty ranges for $\{a_n, \tau_n\}$ are summarised in Table 2. The CO_2 asymptote parameter is expressed through the other exponential weights (Equation 1) and therefore does not have its own uncertainty range. The Monte-Carlo mean and SD for a_0 are 23.4% and 10.0%, respectively.
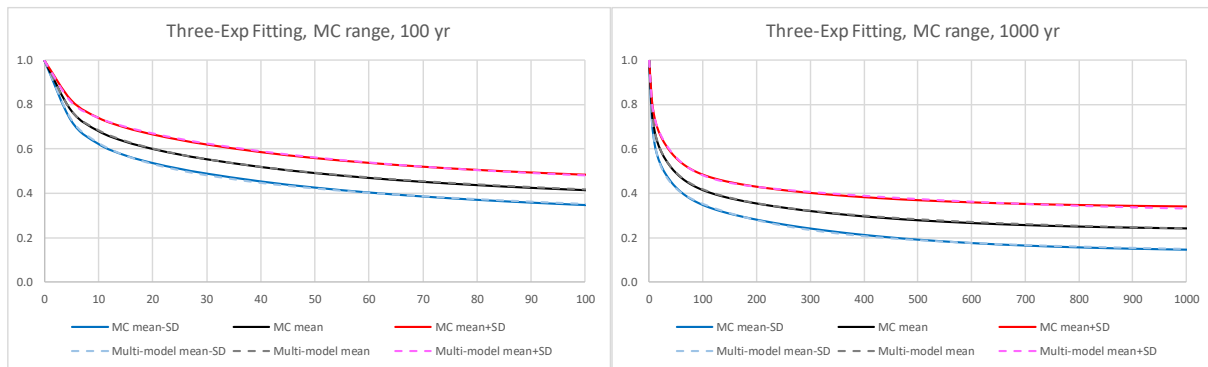
Figure 2. Multi-model mean and ± 1SD range of the CO_2 response function (dashed lines), and the corresponding mean and ± 1SD range of the fitted response function $f(\tau)$ with uncertain parameters $\{a_n, \tau_n\}$ (solid lines), plotted on the timescale of 100 (left) and 1000 (right) years. Source: Joos et al (2013) CO2 cycle calibration 1000 yr horizon.xlsx.

Table 2. Calibration parameters of the CO_2 cycle in PAGE-ICE obtained from statistical fitting to the multi-model CO_2 response function results. Source: Joos et al (2013) CO2 cycle calibration 1000 yr horizon.xlsx.

CO₂ cycle parameters	Min	Mod	Max	Units
Percentage of CO2 long-term ocean uptake (a_1)	4.3	23.0	41.6	%
Percentage of CO2 short-term ocean uptake (a_2)	23.1	26.6	30.1	%
Percentage of CO2 land uptake (a_3)	11.4	27.0	42.5	%
Timescale of CO2 long-term ocean uptake (τ_1)	248.9	312.5	376.2	years
Timescale of CO2 short-term ocean uptake (τ_2)	25.9	34.9	43.9	years
Timescale of CO2 land uptake (τ_3)	2.8	4.3	5.7	years

The response function $f(\tau)$ allows one to find the remaining atmospheric CO_2, $C(t)$, in a given year t associated with anthropogenic emissions from the onset of the pre-industrial era, denoted as t_{00}, by taking convolution of the annual anthropogenic emissions $E(t')$ between t_{00} and t:

$$C(t) = \int_{t_{00}}^{t} E(t') \, f(t - t') dt' \equiv \int_{t_{00}}^{t_0} E(t') \, f(t - t') dt' + \int_{t_0}^{t} E(t') \, f(t - t') dt'$$

Equation 2

The first term on the right hand side represents the contribution of historic emissions between pre-industrial and base year $t_0 = 2015$, while the second term uses a specified emissions scenario for $E(t)$.

Instead of using historic CO_2 emissions records to evaluate the first component in Equation 2, we set $t_{00} = -\infty$ and use the approximation

$$E(t) = E_0 \exp\left(\frac{t - t_0}{\tau_h}\right), \quad t < t_0, \quad \tau_h = \frac{C_0}{E_0}$$

Here $E_0 \approx 41$ GtCO$_2$ per year and $C_0 \approx 2000$ GtCO$_2$ ($\pm 10\%$) are annual and cumulative anthropogenic emissions as of the base year 2015 estimated from the available global records.[9] The exponential approximation for historic emissions gives the following expression for the remaining atmospheric CO_2 under a given future emissions scenario ($t > t_0$):

$$C(t) = \theta C_0 \cdot \left[a_0 + \sum_{n=1}^{3} a_n \cdot \left(\frac{\tau_n}{\tau_h + \tau_n}\right) \cdot \exp\left(\frac{t - t_0}{\tau_n}\right) \right] + \int_{t_0}^{t} E(t') \, f(t - t') dt'$$

Equation 3

Here

$$\theta = \left[a_0 + \sum_{n=1}^{3} a_n \cdot \left(\frac{\tau_n}{\tau_h + \tau_n}\right) \right]^{-1}$$

is a correction compensating for the exponential approximation of the historic emissions, which ensures that $C(t_0) = C_0$.

For the calculations with the PCF, we add an estimate for the cumulative permafrost CO_2 emissions $C_0^{(p)}$ in the base year obtained from SiBCASA to the relevant anthropogenic cumulative emissions C_0, and then add annual permafrost CO_2 emissions $E^{(p)}(t)$ from the emulator to the annual anthropogenic emissions $E(t)$ under a given scenario.

Equation 3 is solved in closed form on each of the analysis periods of PAGE-ICE, separately for the 4 components of the response function, assuming constant anthropogenic emissions during the analysis periods. The solution feeds into the RF formula for CO_2.

PAGE-ICE does not model changes in CO_2 land uptake due to warming and increasing atmospheric CO_2 concentrations (Keenan et al., 2016; Fernández-Martínez, 2018), reductions in CO_2 ocean uptake due to warming and increases in CO_2 ocean uptake driven by carbonate alkalinity changes (Omta et al., 2011), and relies on the default form of the Joos et al. CO_2 response function.

---

[9] Source: http://www.metoffice.gov.uk/research/news/2016/the-global-carbon-budget-2016

Other updates to the climate science

ECS, TCR and FRT parameters

The PAGE-ICE calibration of the equilibrium climate sensitivity (ECS, °C) and transient climate response (TCR, °C) parameters follows results from around 30 CMIP5 models, paleo-records and climate models of intermediate complexity featured in the 5th IPCC Assessment Report (IPCC AR5).[10] Quoting the report:

- 'ECS is likely in the range 1.5°C to 4.5°C (high confidence), extremely unlikely less than 1°C (high confidence), and very unlikely greater than 6°C (medium confidence).'

- 'The TCRs of the 30 AR5 CMIP5 models featured in WGI Table 9.5 vary from 1.1°C to 2.6°C, with a mean of slightly over 1.8°C'.

As in PAGE09, ECS in PAGE-ICE is expressed through TCR and the e-folding feedback response time (FRT, yr) of the upper ocean layers to increased RF:

$$ECS = \frac{TCR}{1 - \frac{FRT}{70} \cdot \left(1 - \exp\left(-\frac{70}{FRT}\right)\right)}$$

The uncertainty range of FRT is set to be between 10 to 55 years (average of 28 years) to give the Monte-Carlo mean value of ECS of 2.8°C (5-95% range of 1.7°C to 4.2°C). This is consistent with the multi-model mean presented in IPCC AR5, which is based on paleo-records, CMIP5 simulations and $2xCO_2$ experiments in climate emulators of intermediate complexity. The calibration is summarised in Table 3.

Table 3. Calibration of the climate sensitivity parameters (TCR, ECS) and the e-folding feedback response time of the upper ocean layers (FRT) to increased RF in PAGE-ICE. Source: PAGE-ICE v6.22 Nonlinear Arctic Feedbacks - Default.xlsx.

Climate sensitivity parameters	Min	Mod	Max	Units
TCR	0.8	1.8	2.7	°C
FRT	10	20	55	yr
ECS (function of TCR and FRT)	1.02	2.56	5.95	°C

To provide further justification for our ECS parameterisation, we conducted the transient $2xCO_2$ and $4xCO_2$ and abrupt $4xCO_2$ experiments in PAGE-ICE. The results, presented in Figure 3 and Table 4 are consistent with IPCC AR5 (Tables 9.5 and 9.6, IPCC AR5 WG1).

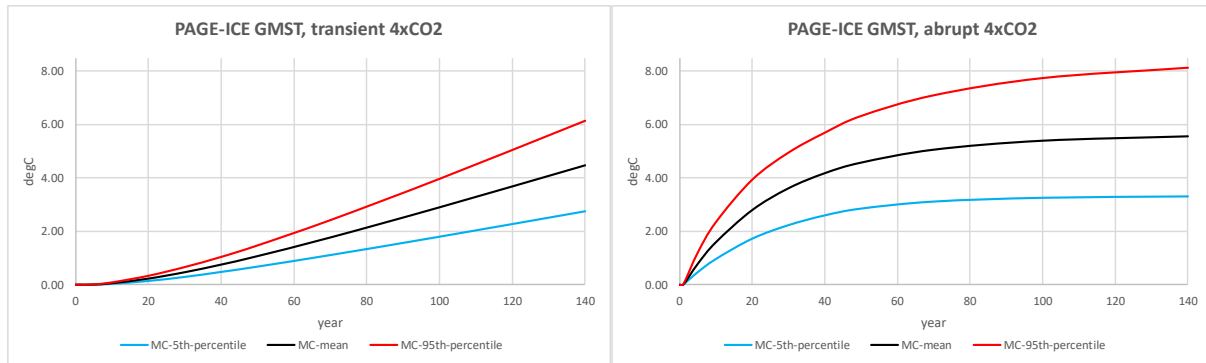[10] https://www.ipcc.ch/pdf/assessment-report/ar5/wg1/WG1AR5_TS_FINAL.pdf

Figure 3. GMST projections (5-95% range and mean) for the transient 2xCO2 and 4xCO2 (left) and abrupt 4xCO2 (right) experiments in PAGE-ICE. Source: PAGE-ICE v6.22 Nonlinear Arctic Feedbacks - Default.xlsx.

Table 4. GMST projections (5-95% range and mean) for the transient 2xCO2 and 4xCO2 and abrupt 4xCO2 experiments in PAGE-ICE after 70 and 140 years. Source: PAGE-ICE v6.22 Nonlinear Arctic Feedbacks - Default.xlsx.

Transient 4xCO2	70 years	140 years
5th percentile	1.1	2.8
Mean	1.8	4.5
95th percentile	2.4	6.2
Abrupt 4xCO2	70 years	140 years
5th percentile	3.1	3.3
Mean	5.1	5.6
95th percentile	7.1	8.1

CMIP5 amplification factors

New probabilistic regional temperature amplification factors (AFs) for the 8 PAGE regions are defined as ratios of the corresponding regional mean surface temperature changes in any given time period to the relevant GMST change, all relative to pre-industrial conditions. The AFs in PAGE-ICE are assumed to be time-independent, and are estimated from CMIP5 multi-model results averaged over the 21st century projections under the four RCP scenarios.

The CMIP5 simulations were driven by time-varying concentrations of GHGs, including aerosols, ozone, as well as GHGs emissions due to land use, volcanic eruptions and solar variability (Taylor et al., 2012). Most models include either semi-interactive or fully interactive aerosol forcing, terrestrial and ocean carbon cycle component and dynamic vegetation, which are key feedbacks of the climate system. In addition, these models include time-evolving ozone field, either prescribed or interactive (Eyring et al., 2013).

The CMIP5 simulations were mainly designed to span the pre-industrial period to the end of the 21st century. The historical simulation run from 1850 to 2005, whereas the future simulations cover the 21st century (2006-2100) and follow the RCP scenarios for GHGs concentrations. Not every model in CMIP5 includes future simulations for all the RCP scenarios. Here we use the CMIP5 results available from the British Atmospheric Data

Centre.[11] All simulations are interpolated to a "common" grid of 2.5º by 1.7º latitude/longitude, which amounts to 278 km by 208 km at the equator.

The AF is associated to the phenomenon that changes in the net radiation balance, for example through increasing GHG concentrations, result in larger (or, in some cases, smaller) changes in the mean surface temperature in multiple world regions compared to the global average, which is particularly pronounced in the Arctic (Alexeev et al., 2005). In any given region, the amplification factor is defined as:

$$AF_r = \frac{\Delta \bar{T}_r}{\Delta \bar{T}}$$

Here $\Delta \bar{T}_r$ is the anomaly in the regional mean surface temperature and $\Delta \bar{T}$ is the corresponding anomaly in GMST, calculated relative to the pre-industrial period (1850-1900), and are averaged over 30-year climatological windows.

To estimate the AFs for each of the 8 regions in PAGE-ICE, we use the CMIP5 ensemble during the 21st Century under the four RCPs emission scenarios. Figure 4 shows the 30-year running mean time series for the AFs from 2021 to 2085. The variations in the AFs both over time and between different RCP scenarios are small in most regions apart from CA (China and South-East Asia), which justifies the use of time-independent AFs in PAGE-ICE. Figure 4 includes boxplots for each individual region to gauge the multi-model mean AFs averaged over the 21st century, separately for each RCP scenario, as well as their associated uncertainties. We use the corresponding multi-scenario boxplots to define the time-independent uncertainty ranges of the AFs in PAGE-ICE, which are given in Table 5.

PAGE-ICE generates its own projections for the GMST change T_t relative to pre-industrial conditions in a future analysis year t under a specified emissions scenario using a simple energy balance model (see below). The corresponding regional temperature anomalies relative to pre-industrial, $T_{r,t}$, are then evaluated using the CMIP5-derived AFs from Table 5:

$$T_{r,t} = T_t \cdot AF_r$$

Equation 4

Table 5. Probability ranges for the AFs in the 8 regions of PAGE-ICE based on the CMIP5 multi-model and multi-RCP data over the 21st century (moving 30-year climatological windows). Units: °C regional per °C global. Source: AF-metrics_CMIP5_ RCPs.xls.

PAGE-ICE Regions	Min	Mod	Max
EU	1.05	1.23	1.53
US	1.16	1.32	1.54
OT	1.14	1.21	1.31
EE	1.41	1.64	1.9
CA	1	1.21	1.3
IA	0.84	1.04	1.15
AF	0.99	1.22	1.42
LA	0.9	1.04	1.18

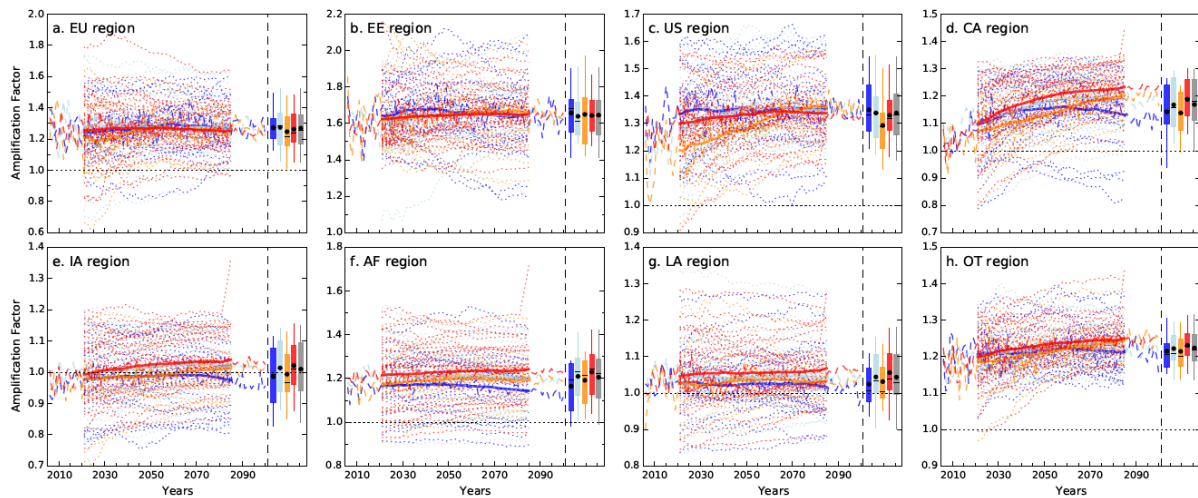[11] ftp://ftp.ceda.ac.uk/badc/cmip5/data.

Figure 4. Amplification factor 30-year running mean time series from 2021 to 2085 for the 8 regions of the PAGE model: (a) European Union, (b) Russia and the rest Eastern Europe (non-EU), (c) United States, (d) China and South-East Asia, (e) India and South Asia, (f) Africa, (g) Latin America and (h) Other OECD countries. The multi-model mean is represented by a solid line and individual models by dotted lines for the RCP2.6 (blue), RCP4.5 (cyan) RCP6.0 (orange) and RCP8.5 (red), respectively. The combined uncertainty over the CMIP5 ensemble and over the time range is represented by the box, whiskers and line, which indicate the interquartile range, 95% range and median, respectively. The corresponding means are indicated by dots. The multi-scenario mean (RCP-2.6-4.5-8.5) is shown in grey. Source: af_timeseries_data.py.

Equation for GMST based on global energy conservation

PAGE-ICE is different from PAGE09 in the ways both the GMST and regional mean surface temperatures are calculated. It uses global average RF from all the 6 policy gases including sulphates to evaluate the GMST first, and then scales the GMST to the regional temperatures using the AFs. Regional RFs from sulphates are no longer used directly due to the following reasons:

- Climatic response to regional RF is characterised by complex heat exchange mechanisms in the Earth's climate system (Shindell & Faluvegi, 2009). Therefore, it is no longer deemed possible to apply the global ECS parameter to translate regional RF into regional temperature anomalies, as was done in PAGE09;
- The regional temperature scaling based on the AFs already includes the regional RF effects implicitly. Adding the RF from sulphates to the regional temperature equations on top of the AFs would lead to double-counting;
- The new implementation preserves the global energy balance.

The governing equation for the realised GMST, denoted as T, is

$$\frac{dT}{dt} = \frac{1}{\text{FRT}} \cdot \left[T_{eq}(t) - T \right], \quad T_{eq}(t) = \frac{\text{ECS}}{F_{sl} \ln 2} \cdot F^{ant}(t)$$

Equation 5

Here $T_{eq}(t)$ is the equilibrium GMST corresponding to a given total anthropogenic RF $F^{ant}(t)$ in analysis year t, which includes globally averaged RFs from all the 6 policy gases in the PAGE model:

$$F^{ant} = F^{CO2} + F^{CH4} + F^{N2O} + F^{Lin} + F^{Sulph} + F^{Exc}$$

F_{sl} (W/m²) is the RF slope parameter for the logarithmic CO_2 RF law (Hope, 2006), and the ECS and FRT parameters are introduced above

Equation 5 is a standard exponential lagged model for the greenhouse effect, which recognises the delay in the upper oceans' warming in response to the RF imbalance. In PAGE-ICE this equation is solved in closed form during each analysis period $t_{i-1} < t < t_i$ using an improved technique based on the following extrapolation for the RF:

$$F^{ant}(t) = F^{ant}_{i-1} + \left(\frac{F^{ant}_{i-1} - F^{ant}_{i-2}}{t_{i-1} - t_{i-2}} \right) \cdot (t - t_{i-1}), \quad t_{i-1} \leq t < t_i$$

The resulting closed-form solution of Equation 5 is

$$T_i = T_{i-1} + (A_{i-1} - \mathrm{FRT} \cdot B_{i-1} - T_{i-1}) \cdot [1 - \mathrm{EXP}_i] + \Delta t_i \cdot B_{i-1}$$

Equation 6

where

$$A_{i-1} = \frac{\mathrm{ECS}}{F_{sl} \ln 2} \cdot F^{ant}_{i-1}, \quad B_{i-1} = \frac{\mathrm{ECS}}{F_{sl} \ln 2} \cdot \left(\frac{F^{ant}_{i-1} - F^{ant}_{i-2}}{t_{i-1} - t_{i-2}} \right),$$

$$\Delta t_i = t_i - t_{i-1}, \quad \mathrm{EXP}_i = \exp\left(-\frac{\Delta t_i}{\mathrm{FRT}} \right)$$

The GMST change T_t in year t described by Equation 6 is then scaled to regional mean surface temperature anomalies $T_{r,t}$ using Equation 4, which are subsequently used to drive economic and non-economic impacts; the GMST change drives SLR and discontinuity impacts. The global mean land surface temperature anomaly $T_{L,t}$ is given by

$$T_{L,t} = \frac{1}{\mathrm{AREA}_L} \left(\sum_r T_{r,t} \cdot \mathrm{AREA}_r \right)$$

where $\mathrm{AREA}_L = 148$ million km² is the total area of the continents of Earth, equal to the sum the areas AREA_r of all the 8 PAGE regions. The global mean ocean surface temperature anomaly is calculated from T_t and $T_{L,t}$ according to the definition of GMST:

$$T_{O,t} = \frac{T_t \cdot \mathrm{AREA}_E - T_{L,t} \cdot \mathrm{AREA}_L}{\mathrm{AREA}_E - \mathrm{AREA}_L}$$

with $\text{AREA}_E = 510$ million km^2 is the total area of the Earth's surface. PAGE-ICE does not utilise $T_{O,t}$ since the model does not account for marine-specific impacts such as ocean acidification.

Global mean and regional mean surface temperature anomalies in the base year

The realised GMST anomaly in the base year 2015, T_0, is defined according to the estimated average climatology around 2015 relative to pre-industrial conditions (1850-1900), based on the EEA and NOAA temperature records.[12] T_0 has the mean value of 0.95°C and uncertainty range of ±0.05°C. The realised regional land temperature anomalies in the base year for each region r of PAGE-ICE, $T_{r,0}$, are evaluated using the corresponding realised GMST combined with the regional amplification factors from CMIP5 models introduced in the section above:

$$T_{r,0} = T_0 \cdot AF_r$$

Their area-weighted mean across the entire land area is equal to

$$T_{L,0} = \frac{1}{\text{AREA}_L} \sum_r T_{r,0} * \text{AREA}_r$$

Initialising the regional temperature anomalies in the base year through the corresponding GMST in the base year and the AFs has a number of advantages:

- A greater consistency with the way the regional temperatures are evaluated in all the analysis years of PAGE-ICE (Equation 4);
- A more balanced estimate given greater natural variability in the regional mean surface temperatures compared with the GMST, which makes it harder to come up with credible base year estimates for the regional temperatures using historic records (as was done in PAGE09);
- A reasonable land-to-ocean temperature increase ratio consistent with historic data.

Fat-tailed distribution for sea level rise based on Nauels et al. (2017)

To utilize the explicit representation of sea level rise (SLR) impacts in PAGE and avoid double-counting of the discontinuity-type impacts attributed to the accelerated decline of Greenland and West Antarctica ice sheets, we introduce Gamma distribution for the time constant τ_{SLR} of SLR in the governing equation

$$\frac{d\,\text{SLR}}{dt} = \frac{\text{SLR}_{eq}(T) - \text{SLR}}{\tau_{SLR}}$$

Here

---

[12] EEA: https://www.eea.europa.eu/data-and-maps/indicators/global-and-european-temperature-4/assessment, NOAA: https://www.ncdc.noaa.gov/cag/global/time-series/globe/land_ocean/ytd/12/1880-2016

$$\text{SLR}_{eq}(T) = \text{SENS}_{SLR} \cdot T + \text{SLR}_{\infty}$$

is the equilibrium SLR expressed as a linear function of the GMST anomaly; SENS_{SLR} is the sensitivity of SLR to GMST changes, and SLR_{∞} is the asymptotic value corresponding to pre-industrial conditions, which takes into account climatic conditions in the past 2000 years (Grinsted et al., 2009).

We use the latest estimate for global SLR percentiles in 2100 under the SSP5 scenario emissions from Nauels et al. (2017) with extra Antarctic ice sheet discharge to calibrate the Gamma distribution parameters for τ_{SLR}. Based on Figure 5 in this reference, the approximate percentile values adjusted to 2015 SLR level are 0.9m (17th), 1.25m (median) and 1.8m (83rd). Running @Risk Optimiser to minimise the root mean square misfit between these percentiles and the corresponding percentiles for the SLR projections in 2100 under RCP8.5 in PAGE-ICE, we find an optimal shape of Gamma distribution for τ_{SLR} plotted in Figure 5 with the following parameters:

<div align="center">Mode = 362 years,   Mean = 386 years</div>

These values correspond to the 'shape' $k = \text{Mean}/(\text{Mean} - \text{Mode}) = 16$ and 'scale' $\theta = (\text{Mean} - \text{Mode}) = 24$ years in the canonical form. The Gamma distribution for τ_{SLR} is equivalent to a fat-tailed distribution for the relative rate of sea level rise,

$$\lambda_{SLR} = \frac{1}{\tau_{SLR}}$$

with the negative algebraic decay power of $-(1 + k) = -17$ at the high-value end (corresponding to rapid SLR response to GMST increases). The Monte-Carlo mean of the resulting SLR in 2100 under the high fossil fuels use scenario (RCP8.5) is 1.57m above pre-industrial levels, which is around 50% higher than the estimate in IPCC AR5 and accounts for recent studies that suggest a possibility of a more rapid collapse of the ice sheets (Golledge et al., 2015; Hansen et al., 2016; Le Bars et al., 2017; Nauels et al., 2017). The calibration of the SLR parameters in PAGE-ICE is summarised in Table 6.

The discontinuity impacts in PAGE-ICE no longer include the risks of catastrophic sea level rise due to the collapse of the ice sheets, and therefore these impacts are downscaled significantly compared with PAGE09 (see below).

Table 6. Calibration of the SLR driver in PAGE-ICE. The probability parameters for the time constant τ_{SLR} of SLR are obtained from 100,000 Monte-Carlo simulations. Source: PAGE-ICE v6.22 Nonlinear Arctic Feedbacks - Default.xlsx.

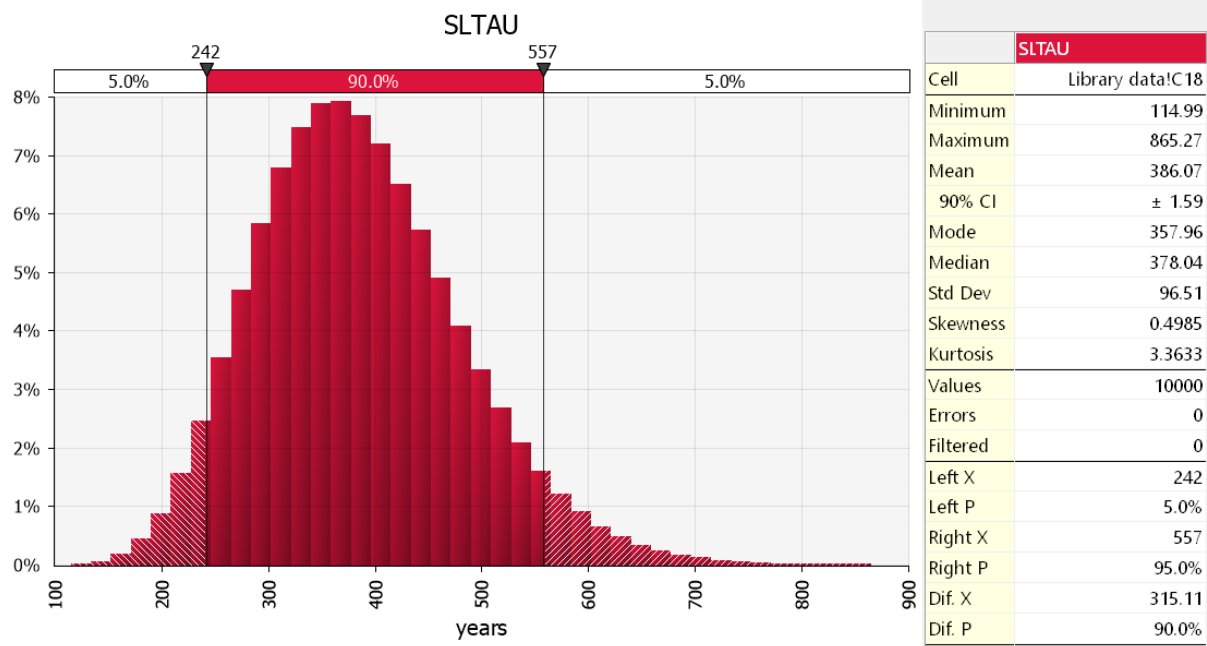| SLR driver parameters	Min	Mod	Max	Units
Sensitivity to GMST changes	0.7	1.5	3	m/°C
Asymptote for pre-industrial	0.5	1	1.5	m
Time constant (Gamma distrib.)	115	362	865	yr

Figure 5. Gamma distribution for the SLR lag parameter τ_{SLR} calibrated using the Nauels et al. (2017) SLR projections. Source: PAGE-ICE v6.22 Nonlinear Arctic Feedbacks - Default.xlsx.

Updates in the economics and policy assumptions

Uncertainty in BAU emissions

PAGE-ICE uses RCP8.5 as the high-end emissions scenario which is referred to as BAU in terms of calculating the mitigation costs. However, there is a considerable uncertainty in long-term emissions projections without climate policies, which is in part due to the nature of technological progress in renewable energy. Estimates suggest that the current BAU trajectory is set to reach 4.2°C by 2100,[13] which is less than the 4.8°C predicted for RCP8.5 by CMIP5 simulations (Knutti and Sedlacek, 2013). However, a recent study of the upper end of the range of SSP emissions indicates that a pathway exceeding RCP8.5 is still a possibility (Christensen et al., 2018). As a result, the parameter of the PAGE model describing the uncertainty in the long-term BAU projections has been adjusted according to the difference between emissions levels in 2100 under the pathway exceeding RCP8.5 and RCP6.0 scenario.[14] This is translated to the values of the "Uncertainty in BAU in 2100" parameter for the four main policy gases in PAGE-ICE relative to the RCP8.5 emission levels summarised in Table 7.

Table 7. Uncertainty in BAU parameter for the four main policy gases in PAGE-ICE. Units: emission levels measured as percentage changes from the corresponding RCP8.5 emissions levels in 2100. Source: PAGE-ICE v6.22 Nonlinear Arctic Feedbacks - Default.xlsx.

Policy gases	Min	Mod	Max
CO_2	-50%	-22%	6%

---

[13] https://www.climateinteractive.org, accessed on 09 September 2017

[14] See the RCP Database, https://tntcat.iiasa.ac.at/RcpDb/dsd?Action=htmlpage&page=compare

CH₄	−67%	−30%	6%
N₂O	−20%	−7%	6%
Linear[15]	−50%	0%	+50%

This scaling is crucial for ensuring that the mitigation costs under all the six climate scenarios considered in the paper are not under- or over-estimated.

Discontinuity impact sector

The discontinuity impact sector in PAGE-ICE accounts only for the possible socio-economic tipping points such as pandemics, mass migration and wars. As a result, the parameters defining the discontinuity impacts have been downscaled considerably compared with PAGE09. The calibration of the discontinuity parameters adopted in PAGE-ICE is given in Table 8. These parameters remain highly uncertain due to the difficulty of modelling the impacts of potentially catastrophic socio-economic events, and therefore the discontinuity calibration used in PAGE-ICE ought to be treated as indicative only.

Table 8. Calibration of the parameters defining the discontinuity impact sector in PAGE-ICE. Source: PAGE-ICE v6.22 Nonlinear Arctic Feedbacks - Default.xlsx.

Discontinuity parameters	Min	Mod	Max	Units
Tolerable GMST level	1	1.5	2	°C
Losses if occurred	1	3	5	% of GDP
Timescale of the losses	10	20	30	Yr

MAC curves and technological learning rates

The marginal abatement cost (MAC) curves in PAGE-ICE are calibrated using the International Energy Agency (IEA) World Energy Outlook study (McKinsey & Company, 2009) together with a more recent review aimed at increasing transparency and comparability in the Paris Agreement in multiple world regions (Aldy et al., 2016). The technological learning rates based on growing experience stock are in line with a recent overview of electricity supply technologies (Rubin et al., 2015). Table 9 summarises the PAGE-ICE calibration of the present-day MAC curve and experience-driven technological learning for CO_2, as well as four additional parameters that define the adjustments to the MAC curves for all the GHG expected to occur by 2100 relative to 2015. The latter include changes to emissions cutbacks at negative costs, increases to maximum cutback through measures such as reforestation, and autonomous technological change approximated using autonomous energy efficiency improvements from the IEA Energy Technology Perspectives study (IEA, 2012). This calibration accounts for the technological progress in energy generation, and is applicable across a wide range of mitigation levels, including those at the deep mitigation end, compatible with achieving the 1.5 and 2°C targets from the Paris Agreement.

---

[15] This category of GHG has multiple components with no clear direction of change from RCP8.5 to RCP6.0 in 2100, so substantial changes in both directions are possible.

Table 9. PAGE-ICE calibration of MAC curves and experience-based learning rates for CO_2 (first five parameters), and additional adjustments to the MAC curves for all the GHG expected to occur by 2100 relative to 2015 (last four parameters). Source: PAGE-ICE v6.22 Nonlinear Arctic Feedbacks - Default.xlsx.

CO_2 MAC curve parameters	Min	Mod	Max	Units
Cutbacks at negative cost	0	10	20	% of emiss.
Most negative cost cutback	−150	−100	−50	$ / Mton
Max cutbacks at positive cost	50	60	70	% of emiss.
Maximum cutback cost	100	150	200	$ / Mton
Learning for 2xExperience stock	0.05	0.2	0.35	fraction drop
General MAC curve evolution	**Min**	**Mod**	**Max**	**Units**
Cutback at negative cost in 2100	0.6	0.9	1.15	vs 2015
Most negative cost in 2100	0.8	0.9	1.1	vs 2015
Maximum cutback in 2100	1	1.1	1.25	vs 2015
Autonomous change in 2100	0.6	0.65	0.7	vs 2015

Economic impact function from Burke et al. (2015)

The PAGE model has four impact sectors: SLR, economic, non-economic and discontinuity. Along with mitigation and adaptation spending, they contribute to the total economic effect of climate change. Compared with PAGE09, PAGE-ICE includes updates to the physical SLR drivers, but not to the economic evaluation of the associated SLR impacts. The discontinuity impacts have been re-defined in line with the updates to the SLR driver and the inclusion of the Arctic land permafrost, land snow and sea ice feedbacks. The now contain only large-scale socio-economic effects of climate change, as well as tipping elements in the climate system other than the nonlinear Arctic feedbacks which are modelled explicitly. The non-economic impacts (gradual changes in ecosystems services and public health not related to the economic output directly) have been updated according to IPCC AR5 (WG2, Chapter 10). We assume that all impacts saturate if they cause GDP losses beyond those seen at the height of the Great Depression in the US in 1933 (around 30% of GDP, or 25% of consumption).[16]

In addition to all the updates described in the previous sections, the improvements in PAGE-ICE have focused on the economic impacts sector, which represent all the climate-driven effects on the economic output apart from those due to SLR and social discontinuities. The economic impacts are driven by changing mean annual temperatures, and are estimated according to recent macro-econometric analysis of historic temperature shocks on economic growth in multiple countries by Burke et al. (2015), the most comprehensive of its kind to date. We projected the Burke et al. impact function onto the 8 major regions of the PAGE model, and adapted it to fit with the single year consumption-only approach for climate impacts known as level effects, as opposed to growth effects (Piontek et al., 2018). This approach provides a conservative estimate for the climate impacts globally.

According to Burke et al., the GDP per capita in a given country with and without the climate effects, denoted respectively as Y and $Y^{(ctrl)}$, changes according to

---

[16] https://www.measuringworth.com/datasets/usgdp/

$$\begin{cases} \dfrac{d \ln Y}{dt} = \eta(t) + \delta(T(t), T_0) \\ \dfrac{d \ln Y^{(ctrl)}}{dt} = \eta(t) \end{cases},$$

Equation 7

Here $\eta(t)$ is the GDP growth rate as per the chosen SSP scenario, which is determined by the SSP-specific set of assumptions on the socio-economic and technological drivers in the given country, and $\delta(T, T_0)$ is the climate correction to the growth rate, which depends on how much the absolute temperature T in this country, measured in ℃, changes relative to its base year value T_0:

$$\delta(T) = h(T) - h(T_0);$$

Here $h(T)$ is the Burke et al. global nonlinear impact function which has the form

$$h(T) = \beta_0 + \beta_1 \cdot T + \beta_2 \cdot T^2 \equiv \gamma_0 + \gamma_1 \cdot (T - T_{cal}) + \gamma_2 \cdot (T - T_{cal})^2$$

$$T_{cal} = 21℃$$

Equation 8

The parameters $\gamma_{1,2,3}$ are all probabilistic, and their values are based on the probability ranges for β_1 and β_2 obtained from the multi-country regression in Burke et al. and listed in their Extended Data Table 1. T_{cal} is the point on the curve with the least uncertainty. The base case estimates for β_1 and β_2, referred to as the "main specification" in Burke et al., correspond to short-term growth effects and are summarised in Table 10.

Table 10. Main specification values of the regression parameters β_1 and β_2 for the economic impact function from Burke et al. (see their Extended Data Table 1, column 1). Source: Burke et al (2015) economic impact function.xlsx.

Parameter	mean	SD	units
Temp. coefficient, β_1	0.0127	0.0038	1/yr per ℃
Temp. squared coefficient, β_2	-0.0005	0.0001	1/yr per (℃)^2

The simulated mean and ±1 SD range of the impact function $h(T)$ described by Equation 8 with the values from Table 10 are plotted in Figure 6. We note that T and T_0 are absolute temperatures in a given country or economic bloc (for example, a region in the PAGE model) and not the anomalies relative to pre-industrial conditions. Also note that although the historic data used by Burke et al. does not have any points beyond $T = 30°$C, we opt to extrapolate the quadratic function to higher temperatures to preserve the pattern of increasing SCCO2 with emissions. As was mentioned earlier, PAGE-ICE has a generic saturation mechanism for the combined impacts of climate change, in which the impacts' limit is set to be of the order of the estimated US GDP loss at the height of the Great Depression. This mechanism is sufficient for capturing the possible saturation of the economic impacts when multiple regional temperatures exceed 30°C (this occurs under high emission scenarios).

Using Equation 7, and following Burke et al., we defined the economic impact function as the percentage difference in the GDP in year t_i due to climate change relative to the "control" GDP without climate change:

$$I(t_i) = \frac{Y^{(ctrl)}(t_i) - Y(t_i)}{Y^{(ctrl)}(t_i)} = 1 - \exp\left(\int_{t_i-\Delta t}^{t_i} \delta(T(t'), T_0)\, dt'\right).$$

Equation 9

Here Δt is the period prior to t_i during which the climate-driven impacts on economic growth have direct influence on the GDP in year t_i, causing the divergence in the GDP trajectories captured by the impact function. If the integral is negative, the impact function is positive (economic losses), while positive values of the integral imply negative impact function (economic gains).

Burke et al. set $\Delta t = t_i - t_0$, therefore assuming that the integral in Equation 9 is taken from t_0 to t_i, i.e. the "memory effects" of climate impacts on economic growth go back to the base year. This interpretation is in line with the shot-term growth effects (but not persistent growth effects, which cause even larger long-term GDP losses). However, after performing lagged regressions for up to 5 years, Burke et al. concluded that: "while we can clearly demonstrate that there is a nonlinear effect of temperature on economic production, we cannot reject the hypothesis that this effect is a true growth effects nor can we reject the hypothesis that it is a temporary level effect" (Burke et al., 2015, Supplementary Materials, p15).
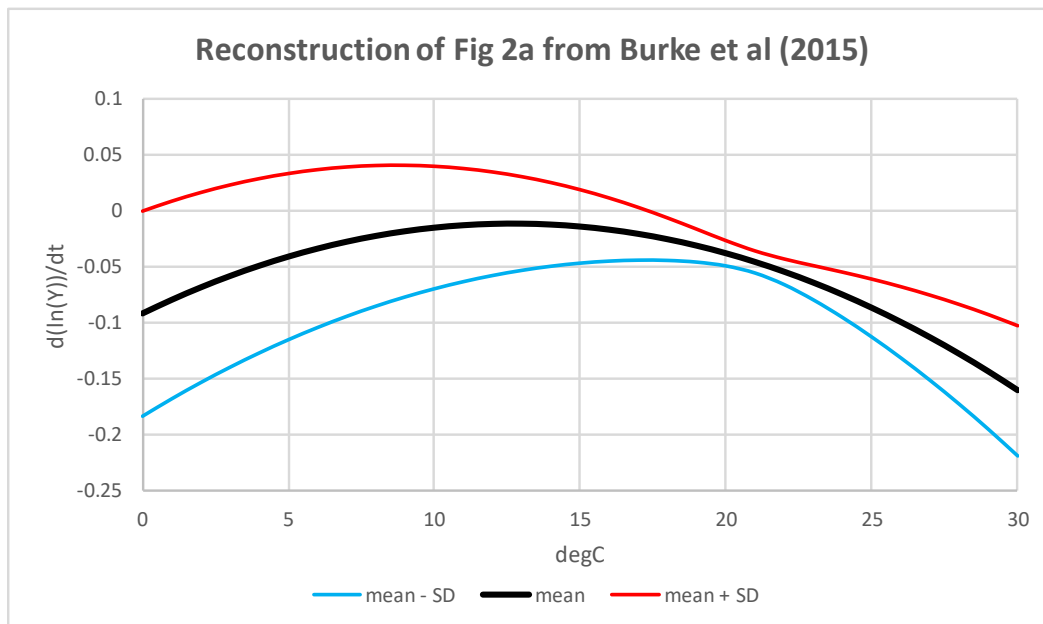
Figure 6. Economic impact function from Burke et al. expressed in terms of the absolute temperature in °C, reconstructed using 10,000 Monte-Carlo simulations of Equation 8. Source: Burke et al (2015) economic impact function.xlsx.

Our understanding is that a given country could experience either the level effects, short-term growth effects or persistent growth effects associated with climate impacts on economy, as per the distinction in Burke et al. (Extended Data, Fig. 2a). Moreover, the nature of response to climate stressors may even switch between the three different options over time. This will depend on each country's unique set of socio-economic policies, as well as global economic trends, which are set to determine its vulnerability and resilience to climate impacts.

In PAGE-ICE, however, we use a more conservative assumption that all the climate-driven losses (gains) are fully repaired (spent on consumption) in the end of each year, which corresponds to the level effects. This implies that $\Delta t = 1$ in Equation 9, and therefore the impacts do not propagate beyond the year during which they occur, giving the following impact function:

$$I(t_i) = 1 - \exp\left(\int_{t_{i-1}}^{t_i} \delta(T(t'), T_0) \, dt' \right).$$

Equation 10

The implication is that in the end of each year the economy rebounds to the same trajectory it was on prior to the losses (gains) occurring in that year. This is in line with the default approach to climate impacts in the PAGE model, which is based on level effects rather than growth effects, and provides an incremental change in the modelling framework, also allowing one to compare directly with the PAGE09 default impact function.

Most importantly, our preference towards the level effects approach is driven by the desire to be able to provide the lowest possible estimate for the impacts of climate change that is unlikely to be reduced further, regardless of the nature of the individual countries' response to future climate stressors.

The base-year absolute temperatures in each of the 8 PAGE regions (Table 11), required for initialising the Burke et al. function, are obtained from Era-Interim re-analysis between 1979 and 2005,[17] and are weighted over population count in each cell.[18] They are adjusted to the PAGE base year climatology using the EEA and NOAA temperature records.[19]

Table 11. PAGE-ICE calibration of climate-driven economic impacts based on the Burke et al. study (short-run specification with one-year regressions), including the mean regional population-weighted temperatures in the 8 PAGE regions corresponding to the 1979-2005 climatology (CMIP5 base period). Source: Burke et al (2015) economic impact function.xlsx, tas_pop-weighted-yr2010_ERA-Interim_PAGE-reg_climo_lowess-smoothing_197901-200512.xlsx.

Consumption share of GDP	75	80	85	% of GDP
Linear temperature coefficient, γ_1	-1.40E-02	-8.30E-03	-2.62E-03	1/yr per ºC
Quadratic temperature coefficient, γ_2	-6.00E-04	-5.00E-04	-4.00E-04	1/yr per (ºC)^2
Impacts saturate beyond	15	20	25	% consum.
Mean regional temperatures, 1979-2005 climatology:				
EU	6.762315	10.1222	13.48209	ºC
US	9.542101	13.42862	17.31514	ºC
Other OECD	9.075961	12.06335	15.05075	ºC

---

[17] https://www.ecmwf.int/en/forecasts/datasets/archive-datasets/reanalysis-datasets/era-interim
[18] Gridded population map from http://sedac.ciesin.columbia.edu/data/set/gpw-v4-population-count-rev10/data-download
[19] EEA: https://www.eea.europa.eu/data-and-maps/indicators/global-and-european-temperature-4/assessment, NOAA: https://www.ncdc.noaa.gov/cag/global/time-series/globe/land_ocean/ytd/12/1880-2016

FSU	3.013205	7.113213	11.21322	ºC
CA	12.23304	15.01296	17.79287	ºC
IA	23.38633	24.94998	26.51362	ºC
Af & ME	20.18669	21.89225	23.59781	ºC
LA	19.48468	21.1204	22.75611	ºC

Complete list of the uncertain parameters in PAGE-ICE

Table 12 provides complete list of the uncertain parameters in PAGE-ICE. Unless otherwise stated, all the parameters are approximated by triangular distributions defined by the min, mod and max values stated in the table. A small number of parameters in Table 12 such the 2xCO2 equilibrium climate sensitivity (ECS) or the autonomous technological progress rate are expressed as functions of one or more "primary" parameters with triangular distributions. The time constant of sea level rise is approximate by Gamma distribution. Further comments are provided in the Excel workbook of PAGE-ICE.

Table 12. Complete list of the uncertain parameters in PAGE-ICE. Source: PAGE-ICE v6.22 Nonlinear Arctic Feedbacks - Default.xlsx.

Parameter	mean	min	mod	Max	units
Discount rates and base year climatology					
PTP rate	1.033	0.1	1	2	% per year
Elasticity of utility	1.167	0.5	1	2	
Base year cumulative CO2 emissions	2035	1833	2035	2237	Gton CO2
Base year GMST anomaly from pre-ind.	0.95	0.90	0.95	0.99	degC
Absolute GMST in each region, population-weighted, CMIP5 base period climatology					
EU	10.12	6.76	10.12	13.48	degC
US	13.43	9.54	13.43	17.32	degC
Other OECD	12.06	9.08	12.06	15.05	degC
FSU	7.11	3.01	7.11	11.21	degC
China & CP Asia	15.01	12.23	15.01	17.79	degC
India and SE Asia	24.95	23.39	24.95	26.51	degC
Africa and ME	21.89	20.19	21.89	23.60	degC
Latin America	21.12	19.48	21.12	22.76	degC
Base year cumulative permafrost emissions					
Base year cumulative carbon, permafrost CO2	4190.01	3.83E+03	4.12E+03	4.62E+03	MtonC
Base year cumulative carbon, permafrost CH4	180.3806	1.75E+02	1.80E+02	1.86E+02	MtonC
CO2 cycle					

Percent of CO2 long-term ocean uptake	22.97	4.3	23.0	41.6	%
Percent of CO2 short-term ocean uptake	26.64	23.1	26.6	30.1	%
Percent of CO2 land uptake	26.96	11.4	27.0	42.5	%
Timescale of CO2 long-term ocean uptake	312.54	248.9	312.5	376.2	years
Timescale of CO2 short-term ocean uptake	34.87	25.9	34.9	43.9	years
Timescale of CO2 land uptake	4.26	2.8	4.3	5.7	years
Sulphate aerosols					
Sulfate direct (linear) effect in 2015	-0.47	-0.8	-0.4	-0.2	W/m2
Sulfate indirect (log) effect for a doubling of sulphates	-0.23	-0.5	-0.2	0	W/m2
Sea level rise					
Sea level rise in 2015	0.19	0.17	0.19	0.21	m
Sea level rise with temperature	1.73	0.7	1.5	3	m/degC
Sea level asymptote	1.00	0.5	1	1.5	m
Time constant of sea level rise (*Gamma*)	386		362		years
Climate sensitivity					
Transient climate response	1.77	0.8	1.8	2.7	degC
Feedback response time	28.33	10	20	55	years
Equilibrium warming for a doubling of CO2	2.81	Function of TCR and FRT			degC
Regional amplification factors					
EU amplification factor	1.27	1.05	1.23	1.53	
US amplification factor	1.34	1.16	1.32	1.54	
OT amplification factor	1.22	1.14	1.21	1.31	
EE amplification factor	1.65	1.41	1.64	1.9	
CA amplification factor	1.17	1	1.21	1.3	
IA amplification factor	1.01	0.84	1.04	1.15	
AF amplification factor	1.21	0.99	1.22	1.42	
LA amplification factor	1.04	0.9	1.04	1.18	
SAF emulator					

Normalised random variable for the emulator	0.00	-1	0	1	dimensionless
PCF emulator					
Uncertainty in the initial carbon stock	0	-15	0	15	%
SiBCASA					
Amplification factor for permafrost regions	1.88	1.43	1.88	2.33	dimensionless
Sensitivity for cumulative carbon emissions, CO2	3.19E+04	2.82E+04	3.19E+04	3.57E+04	MtonC/degC
Time lag for cumulative carbon emissions, CO2	61.69	35.49	61.69	87.89	yr
Nonlinear power for cumulative carbon emissions, CO2	0.26	0.11	0.26	0.41	dimensionless
Sensitivity for cumulative carbon emissions, CH4	2.29E+03	1.24E+03	2.29E+03	3.35E+03	MtonC/degC
Time lag for cumulative carbon emissions, CH4	206.29	75.19	206.29	337.38	yr
Nonlinear power for cumulative carbon emissions, CH4	0.25	-0.11	0.25	0.61	dimensionless
JULES					
Amplification factor for permafrost regions	1.94	1.71	1.94	2.16	dimensionless
Sensitivity for cumulative carbon emissions, CO2	6.19E+04	2.47E+04	6.19E+04	9.90E+04	MtonC/degC
Time lag for cumulative carbon emissions, CO2	543.62	252.56	543.62	834.67	yr
Nonlinear power for cumulative carbon emissions, CO2	0.46	-0.23	0.46	1.14	
Permafrost CH4 carbon relative to CO2 carbon	6.12	2.77	6.04	9.53	%
Impacts of climate change					
Savings rate	15.00	10	15	20	%
Calibration sea level rise	0.50	0.45	0.5	0.55	m
Calibration temperature	3.00	2.5	3	3.5	degC
Impacts saturate beyond	20.00	15	20	25	%consumption

Statistical value of civilisation	6.1E+10	1.15E+10	5.75E+10	1.15E+11	$M(2015)
Sea level rise					
Sea level initial benefit	0.00	0	0	0	%GDP per m
Sea level impact at calibration sea level rise	1.00	0.5	1	1.5	%GDP
Sea level impact function exponent	0.73	0.5	0.7	1	
Sea level exponent with income	-0.30	-0.4	-0.3	-0.2	
Economic					
Economic impact Burke: temp coeff	-8.30E-03	-1.40E-02	-8.30E-03	-2.62E-03	1/yr per degC
Economic impact Burke: temp squared coeff	-5.00E-04	-6.00E-04	-5.00E-04	-4.00E-04	1/yr per degC^2
Non-economic					
Non-econ initial benefit	0.08	0	0.05	0.2	%GDP per degC
Non-econ impact at calibration temperature	0.63	0.1	0.6	1.2	%GDP
Non-econ impact function exponent	2.17	1.5	2	3	
Non-econ exponent with income	0.00	-0.2	0	0.2	
Discontinuity					
Random variable *(uniform)*	0.5	0	N.A.	1	dimensionless
Tolerable before discontinuity	1.50	1	1.5	2	degC
Chance of discontinuity	20.00	10	20	30	% per degC
Loss if discontinuity occurs	3.00	1	3	5	%GDP
Discontinuity exponent with income	-0.13	-0.3	-0.1	0	
Time constant of discontinuity	20.00	10	20	30	years
Weights (sea level)					
US Sea level weights factor	0.80	0.6	0.8	1	
OT Sea level weights factor	0.80	0.4	0.8	1.2	
EE Sea level weights factor	0.40	0.2	0.4	0.6	
CA Sea level weights factor	0.80	0.4	0.8	1.2	

IA Sea level weights factor	0.80	0.4	0.8	1.2	
AF Sea level weights factor	0.60	0.4	0.6	0.8	
LA Sea level weights factor	0.60	0.4	0.6	0.8	
Adaptation costs					
Adaptive costs sea level plateau	0.0233	0.01	0.02	0.04	%GDP per metre
Adaptive costs sea level impact	0.0012	0.0005	0.001	0.002	%GDP per %reduction per metre
Adaptive costs Economic plateau	0.0117	0.005	0.01	0.02	%GDP per degC
Adaptive costs Economic impact	0.0040	0.001	0.003	0.008	%GDP per %reduction per degC
Adaptive costs Non-econ plateau	0.0233	0.01	0.02	0.04	%GDP per degC
Adaptive costs Non-econ impact	0.0057	0.002	0.005	0.01	%GDP per %reduction per degC
Weights (adaptation)					
US Adaptive costs factor	0.80	0.6	0.8	1	
OT Adaptive costs factor	0.80	0.4	0.8	1.2	
EE Adaptive costs factor	0.40	0.2	0.4	0.6	
CA Adaptive costs factor	0.80	0.4	0.8	1.2	
IA Adaptive costs factor	0.80	0.4	0.8	1.2	
AF Adaptive costs factor	0.60	0.4	0.6	0.8	
LA Adaptive costs factor	0.60	0.4	0.6	0.8	
Mitigation costs					
CO2					
Uncertainty in BAU emissions in 2100	-22.00	-50	-22	6	% relative to RCP8.5
Initial cutbacks at negative cost	10.00	0	10	20	% of emissions
Initial most negative cost cutback	-100.00	-150	-100	-50	$M(2015) per Mtonne
Initial maximum cutbacks at positive cost	60.00	50	60	70	% of emissions
Initial maximum cutback cost	150.00	100	150	200	$M(2015) per Mtonne
Initial experience stock	150000.00	100000	150000	200000	Mtonne
CH4					

Uncertainty in BAU emissions in 2100	-30.33	-67	-30	6	% relative to RCP8.5
Initial cutbacks at negative cost	10.00	0	10	20	% of emissions
Initial most negative cost cutback	-4983.33	-9200	-4600	-1150	$M(2015) per Mtonne
Initial maximum cutbacks at positive cost	51.67	35	50	70	% of emissions
Initial maximum cutback cost	7283.33	3450	6900	11500	$M(2015) per Mtonne
Initial experience stock	2000.00	1500	2000	2500	Mtonne
N2O					
Uncertainty in BAU emissions in 2100	-7.00	-20	-7	6	% relative to RCP8.5
Initial cutbacks at negative cost	10.00	0	10	20	% of emissions
Initial most negative cost cutback	-8433.33	-17250	-8050	0	$M(2015) per Mtonne
Initial maximum cutbacks at positive cost	51.67	35	50	70	% of emissions
Initial maximum cutback cost	31433.33	2300	23000	69000	$M(2015) per Mtonne
Initial experience stock	53.33	30	50	80	Mtonne
Linear (HGWP gases)					
Uncertainty in BAU emissions in 2100	0.00	-50	0	50	% relative to RCP8.5
Initial cutbacks at negative cost	10.00	0	10	20	% of emissions
Initial most negative cost cutback	-268.33	-460	-230	-115	$M(2015) per Mtonne
Initial maximum cutbacks at positive cost	70.00	60	70	80	% of emissions
Initial maximum cutback cost	383.33	115	345	690	$M(2015) per Mtonne
Initial experience stock	2000.00	1500	2000	2500	Mtonne
Weights (uncertainty in BAU)					
US uncertainty in BAU emissions factor	1.00	0.8	1	1.2	
OT uncertainty in BAU emissions factor	1.00	0.8	1	1.2	
EE uncertainty in BAU emissions factor	1.00	0.65	1	1.35	
CA uncertainty in BAU emissions factor	1.00	0.5	1	1.5	
IA uncertainty in BAU emissions factor	1.00	0.5	1	1.5	

AF uncertainty in BAU emissions factor	1.00	0.5	1	1.5	
LA uncertainty in BAU emissions factor	1.00	0.5	1	1.5	
Weights (uncertainty in negative mitigation costs)					
US negative cost percentage factor	1.08	0.75	1	1.5	
OT negative cost percentage factor	1.00	0.75	1	1.25	
EE negative cost percentage factor	0.70	0.4	0.7	1	
CA negative cost percentage factor	0.70	0.4	0.7	1	
IA negative cost percentage factor	0.70	0.4	0.7	1	
AF negative cost percentage factor	0.70	0.4	0.7	1	
LA negative cost percentage factor	0.70	0.4	0.7	1	
Weights (uncertainty in maximum adaptation costs)					
US maximum cost factor	1.00	0.8	1	1.2	
OT maximum cost factor	1.23	1	1.2	1.5	
EE maximum cost factor	0.70	0.4	0.7	1	
CA maximum cost factor	1.00	0.8	1	1.2	
IA maximum cost factor	1.23	1	1.2	1.5	
AF maximum cost factor	1.23	1	1.2	1.5	
LA maximum cost factor	0.70	0.4	0.7	1	
Evolution in mitigation costs					
Cutbacks at negative cost in 2100 as multiple of 2015	0.88	0.6	0.9	1.15	
Cutbacks at negative cost growth rate	-0.15	Function of the changes in 2100			% per year
Most negative cost in 2100 as multiple of 2015	0.93	0.8	0.9	1.1	
Most negative cost growth rate	-0.08	Function of the changes in 2100			% per year
Maximum cutbacks in 2100 as multiple of 2015	1.12	1	1.1	1.25	
Maximum cutbacks growth rate	0.13	Function of the changes in 2100			% per year
Curvature below zero cost	0.50	0.25	0.45	0.8	

Curvature above zero cost	0.40	0.1	0.4	0.7	
Experience crossover ratio	0.20	0.1	0.2	0.3	
Learning rate (prop. drop in cost for experience doubling)	0.20	0.05	0.2	0.35	proportional drop
Costs in 2100 as multiple of 2015	0.65	0.6	0.65	0.7	
Autonomous technical change	0.51	Function of the changes in 2100			% per year
Equity weights proportion	1.00	1	1	1	

Emulator for the nonlinear PCF using SiBCASA and JULES simulations

The new dynamic emulator for CO_2 and methane emissions from thawing land permafrost is based on simulations from the SiBCASA and JULES land surface models (LSMs) (Schaefer et al., 2011; Burke et al., 2017), forced by multiple CMIP5 and CMIP3 general circulation models (GCMs) run under a range of climate scenarios out to 2300. The simulated CO_2 and methane fluxes from thawing permafrost as a function of time represent the strength and timing of the PCF.

SiBCASA has fully integrated water, energy, and carbon cycles, and a modified snow model to better simulate permafrost dynamics (Schaefer et al., 2009). The soil model separately tracks liquid water, ice, and frozen organic matter at each time step as prognostic variables, accounting for the effects of latent heat (Schaefer and Jafarov, 2016). SiBCASA separately tracks CO_2 and methane emissions. The model was used to make one of the first estimates of future permafrost degradation and global carbon emissions from thawing permafrost. Here we ran multiple projections from 1901 to 2300 starting from the same initial conditions. We spun up the model until the release from permafrost carbon was negligible, ending up with 560 GtC of frozen permafrost carbon in the top three meters of soil (Schaefer and Jafarov, 2016; Jafarov and Schaefer, 2016) by initializing the model with the observed values from the Northern Circumpolar Soil Carbon Dataset version 2 (NCSCDv2) (Hugelius et al., 2014). We used the Climatic Research Unit National Centre for Environmental Predictions (CRUNCEP) reanalysis (Wei et al., 2014) scaled by global climate projections from CMIP5 (Taylor et al., 2012). We chose CMIP5 models that ran both RCP4.5 and RCP8.5 scenarios out to 2300 and that represent a broad range of warming above pre-industrial temperatures: CNRM-CM5, GISS-E2-H, HadGEM2-ES, IPSL-CM5A-LR and MPI-ESM-LR.

The version of JULES used here has an improved representation of physical and biogeochemical processes in the cold regions (Chadburn et al., 2015; Burke et al., 2017b). Competition of vegetation swas enabled, allowing the models to determine both their initial vegetation distributions and litterfall, and the response of the vegetation distribution and litterfall to climate change. The profile of soil carbon was spun up until it was in equilibrium

with the 1860's climate, giving 738 GtC in the top 3m of soil. Any soil carbon in the permafrost in 1860 was labelled as "permafrost carbon" and traced throughout the simulation. We assumed that any part of this permafrost carbon which is emitted to the atmosphere is emitted in the form of CO_2 only. JULES was forced by climate patterns from the full set of 22 CMIP3 climate model simulations under the RCP2.6, RCP4.5 and RCP8.5 scenarios, extended out to 2300 using the IMOGEN climate emulator (Burke et al., 2017).

The dynamic emulator of the permafrost carbon emissions is based on a nonlinear first order ODE:

$$\frac{dC}{dt} = \frac{C_{max}}{\tau \, \varphi_\tau(T)} \cdot \left(\frac{\max(C_{eq}(T) - C, 0)}{C_{max}} \right)^{(1+p)\, \varphi_p(T)}$$

Equation 11

Here $T = AF_p \cdot \text{GMST}$ is mean annual permafrost temperature anomaly in year t, averaged spatially across the estimated pre-industrial permafrost regions (°C relative to pre-industrial levels); AF_p is the parmafrost amplification factor which links T with the GMST anomaly; C is cumulative permafrost carbon emitted since the pre-industrial period as of time t (GtC, either CO_2 or methane component); $C_{eq}(T)$ is equilibrium cumulative carbon emitted for a constant permafrost temperature anomaly T, expressed as

$$C_{eq}(T) = \min(\omega \, \varphi_\omega(T) \cdot T, C_{max}) \, ;$$

C_{max} is a limit on the maximum possible cumulative emissions determined by the initial carbon stock estimates in SiBCASA (560 GtC) and JULES (738 GtC); ω (GtC K^{-1}) is equilibrium sensitivity of the carbon emissions to permafrost warming; τ (yr) is the time lag at $t = 0$ (pre-industrial) corresponding to the given C_{max}; p is a fixed power that defines the dynamics of how the equilibrium is approached. All the parameters are assumed to be constant unless they are marked as functions. Equation 11 implies no regeneration of permafrost carbon stocks on the timescales considered (Zimov et al., 2006).

The emulator is calibrated, separately, to the CO_2 components of the permafrost emissions simulated by SiBCASA and JULES, and the methane component simulated by SiBCASA. Each combination of a GCM (m) and climate scenario (s), either in SiBCASA or JULES simulations, produces its own set of optimal equilibrium carbon, lag and power parameters $(\omega, \tau, p)_{m,s}$ that achieves the best emulator fit. The resulting statistics for the ω, τ, p parameters is based on the assumptions of equal weights between the GCMs and the scenarios. The φ_ω, φ_τ, φ_p functions (all non-negative) represent temperature corrections to their respective parameters, ensuring quasi-independence of the $(\omega, \tau, p)_{m,s}$ set as a whole from the scenarios or climate models used (Supplementary Materials). The latter allows us to use these sets of values to construct the corresponding probability distributions for ω, τ, p in PAGE-ICE, which are expected to work throughout the simulated range of temperatures.

The type of a model described by Equation 11 is often referred to as "pursuit curve", and its simpler quasi-linear version ($p = 0$) has been employed for sea level rise emulators previously (Grinsted et al., 2009; Mengel et al., 2018). Even in its simpler form, such a model has never been applied to projected permafrost emissions from process-based simulations of LSMs. The pursuit curve model ensures that there is an equilibrium level of cumulative carbon emissions

from permafrost for any given level of warming globally (providing $p > -1$). The dynamic model formulation employed here contains the following layers of nonlinearity: nonlinear response of the equilibrium cumulative carbon to GMST changes, represented by the $\omega \, \varphi_\omega(T) \cdot T$ term; evolution of the characteristic time lag for cumulative permafrost emissions with the difference between the equilibrium and realised cumulative carbon, represented by p (in the corresponding linear model $p = 0$ and the lag is simply equal to τ); temperature-dependence in the lag and power parameters, represented by φ_τ, φ_p; and, saturation of the cumulative carbon emissions due to the permafrost carbon stock exhaustion, represented by C_{max}.

The cumulative carbon emissions from the emulators, calibrated separately to SiBCASA and JULES simulations, were averaged with equal weights, both for CO_2 and methane, and scaled according to the uncertainty in the observed permafrost carbon stocks (Hugelius et al., 2014). As JULES does not model permafrost methane emissions explicitly, the latter were inferred from its CO_2 emissions using observational constraints (Schädel et al., 2016). The resulting cumulative CO_2 and methane emissions from permafrost simulated by PAGE-ICE are plotted in Figure 7 under the range of scenarios considered.
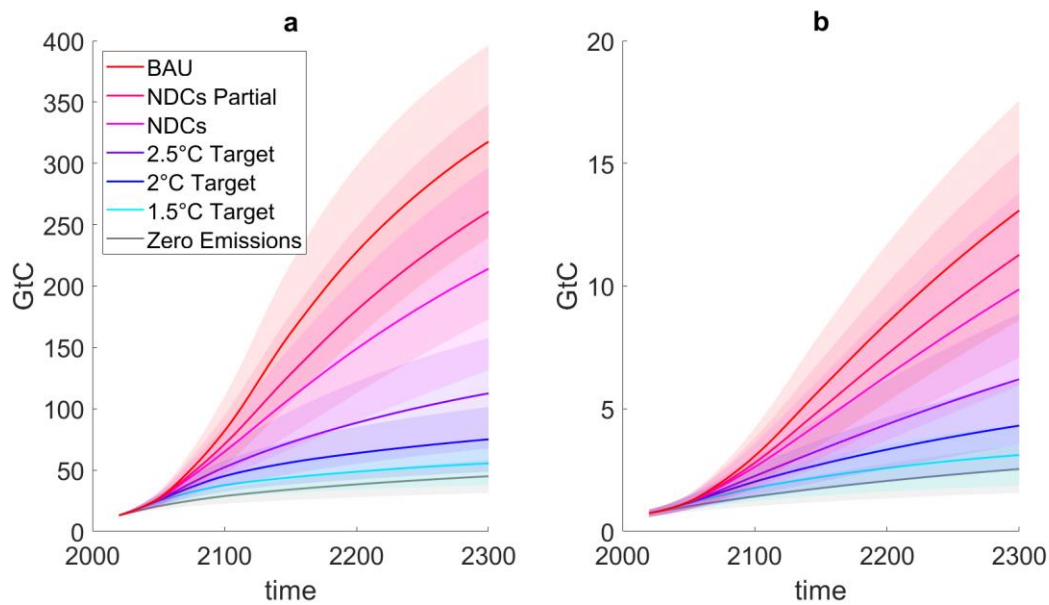
Figure 7. Cumulative carbon emissions from thawing land permafrost for the CO2 (a) and methane (b) components simulated by the new statistical emulator of SiBCASA and JULES (equal weighting) under the chosen range of climate scenarios until year 2300 (solid lines: mean; shaded areas: ±1 SD). 100,000 Monte-Carlo runs of PAGE-ICE. Units: GtC. Note the difference in the Y-axis scale between the plots. Source: Yumashev et al. (2019).

Calibration algorithm for the PCF emulator

We calibrated the emulator separately for the CO_2 and methane fluxes simulated by SiBCASA, and for the CO_2 fluxes simulated by JULES. The simulations of these two LSMs used gridded daily CMIP5 (SiBCASA) or CMIP3 (JULES) projections for temperature and precipitation in the permafrost region, which was defined according to the simulated pre-industrial permafrost extent (1850-1900). The emulator was forced by mean annual GMST projections from the same CMIP5 experiments throughout the fitting procedure. In the emulator runs, the gridded

GMST projections from the CMIP5 models were converted into mean annual temperatures T averaged across the pre-industrial permafrost region using the corresponding amplification factors derived separately for each CMIP5 or CMIP3 model:

$$T = AF_p \cdot \text{GMST}.$$

The emulator calibration involved applying a standard gradient-free "fminsearch" algorithm in MATLAB that minimises a normalised misfit between the LSM simulations and a numerical solution of Equation 14 defining the emulator (below) by adjusting three main parameters: ω, τ, p. The normalised misfit, $\varepsilon_{m,s}$, is defined as

$$\varepsilon_{m,s} = \frac{1}{\max\limits_{m',s'}\left(C_{m',s'}^{LSM}(t_N)\right)} \cdot \left[\frac{1}{N}\sum_{i=1}^{N}\left(C_{m,s}(t_i) - C_{m,s}^{LSM}(t_i)\right)^2\right]^{\frac{1}{2}},$$

Equation 12

where t_i is time, running from 2000 to 2300; $N = 300$ is the number of time steps; $C_{m,s}^{LSM}(t_i)$ is the cumulative carbon flux at time t_i from the LSM simulations (SiBCASA or JULES) with the GCM m under the scenario s; and $C_{m,s}(t_i)$ is the corresponding numerical solution of Equation 14.

Each combination of a GCM and scenario in the LSM simulations produces its own set of optimal parameters $(\omega, \tau, p)_{m,s}$ that minimises $\varepsilon_{m,s}$. It turns out that such a procedure yields inter-scenario biases in the parameters ω, τ, p, where the parameters appear to cluster around different values depending on the scenario. To reduce the biases, we introduced the nonlinear corrections φ_ω, φ_τ, φ_p, which are functions of the permafrost temperature. These were obtained from an iteration algorithm assuming that the optimal parameters $(\omega, \tau, p)_{m,s}$ on each iteration are functions of the relevant permafrost temperatures $T_{m,s}(t_N)$ in year $t_N = 2300$ (end of the timespan for the datasets). The functional forms used for the temperature corrections are:

$$\varphi_{\omega,\tau}(T) = \begin{cases} 1 + \delta_{\omega,\tau} \cdot \left(\dfrac{T - 0.5 \cdot T_{max}}{T_{max}}\right), & \text{SiBCASA CO2} \\[2ex] \left(\dfrac{T}{0.5 \cdot T_{max}}\right)^{\delta_{\omega,\tau}}, & \text{SiBCASA CH4, JULES CO2} \end{cases}$$

$$\varphi_p(T) = 1 + \delta_p \cdot \left(\frac{T - 0.5 \cdot T_{max}}{T_{max}}\right), \quad \text{all cases}$$

Equation 13

Here δ_ω, δ_τ, δ_p are constant dimensionless slopes adjusted on each iteration to reduce the inter-scenario bias, and T_{max} is the highest permafrost temperature anomaly from pre-industrial achieved in the GCM simulations with either SiBCASA or JULES. The adjustments to the slopes were performed by means of an appropriate polynomial fitting between $(\omega, \tau, p)_{m,s}$ and $T_{m,s}(t_N)$. The nonlinear correction δ_ω, for example, is adjusted as follows between two consecutive iterations:

$$\delta_\omega^{(iter)} = \delta_\omega^{(iter-1)} + \mu_\omega \cdot \left(\text{slope}\{\omega_{m,s}, T_{m,s}(t_N)\}\right)^{(iter-1)}$$

Here slope$\{\cdot\}$ is the slope parameter for either a linear (SiBCASA CO_2; $\omega \sim T$) or log-linear (SiBCASA methane and JULES CO_2; $\ln \omega \sim \ln T$) polynomial fitting of the set of values $\omega_{m,s}$ to the set of values $T_{m,s}(t_N)$ across all the models m and scenarios s, and μ_ω is an empirically determined damping factor that makes the iterations converge.[20] For SiBCASA CO_2, we have the following expression for the slope parameter $s_\omega^{(iter)}$:

$$\left\{ \frac{\omega_{m,s}^{(iter)}}{\text{mean}_{m',s'}\left(\omega_{m',s'}^{(iter)}\right)} \right\} = s_\omega^{(iter)} \cdot \left\{ \frac{T_{m,s}(t_N) - 0.5 \cdot T_{max}}{T_{max}} \right\} + \text{fitting residue,}$$

For SiBCASA methane and JULES CO_2, this is modified to

$$\ln\left\{ \frac{\omega_{m,s}^{(iter)}}{\text{mean}_{m',s'}\left(\omega_{m',s'}^{(iter)}\right)} \right\} = s_\omega^{(iter)} \cdot \ln\left\{ \frac{T_{m,s}(t_N)}{0.5 \cdot T_{max}} \right\} + \text{fitting residue,}$$

The iterative adjustments to δ_τ and δ_p follow the same procedure, depending on which functional form is used according to to Equation 13.[21]

The iterations are stopped when each of the relevant correlation coefficients,

$$R^2\{\omega_{m,s}, T_{m,s}(t_N)\}, \quad R^2\{\tau_{m,s}, T_{m,s}(t_N)\}, \quad R^2\{p_{m,s}, T_{m,s}(t_N)\},$$

falls below a required minimum threshold of 0.01,[22] ensuring that the optimal parameter sets $(\omega, \tau, p)_{m,s}$ are quasi-independent from the scenarios or models that were used to obtain them. The latter allows us to use these sets of values to construct the corresponding probability distributions for ω, τ, p in PAGE-ICE, which are expected to work throughout the simulated range of temperatures. This clear statistical criterion implies that our PCF emulator is robust and its range of applicability can be extended to scenarios such as the 1.5°C and 2°C targets (Figure 7). Further technical details of the fitting algorithm and the resulting numerical values are given in the sections below.

CO₂ component, SiBCASA

Figure 8 shows projected cumulative permafrost CO_2 emissions until 2300 under the RCP4.5 and RCP8.5 scenarios, generated by SiBCASA and by our model emulator, individually for each of the five CMIP5 models employed in the SiBCASA simulations. The plots in Figure 8 demonstrate a very good fitting accuracy.

---

[20] $\mu_\omega = 0.5$ SiBCASA CO_2; $\mu_\omega = 0.25$ for SiBCASA methane and JULES CO_2 emulator fitting.

[21] $\mu_\tau = 0.5$, $\mu_p = 0.1$ SiBCASA CO_2; $\mu_\tau = \mu_p = 0.25$ for SiBCASA methane and JULES CO_2 emulator fitting.

[22] Established empirically to allow for convergence of the iterations to calibrate the emulator, separately, to the SiBCASA CO_2, SiBCASA methane and JULES CO_2 simulations.

Figure 9 shows the time-constant fitting parameters $(\omega, \tau, p)_{m,s}$ for the CO_2 component of the PCF emulator for all the models m and scenarios s, plotted against the relevant permafrost temperature projections $T_{end} = T_{m,s}(t_N)$ in year $t_N = 2300$ (end of the timespan for the datasets). The values $(\omega, \tau, p)_{m,s}$ are obtained through minimising the normalised misfit between the SiBCASA and emulator projections for the cumulative carbon emissions plotted in Figure 8. They are adjusted further in a special iteration algorithm that minimises the inter-scenario bias, as is described in the section above. The residual correlations between $(\omega, \tau, p)_{m,s}$ and $T_{m,s}(t_N)$ are close to zero.

Figure 10 shows how the correlation coefficients and the corresponding slopes δ_ω, δ_τ, δ_p, which define the temperature-dependent corrections φ_ω, φ_τ, φ_p to the parameters ω, τ, p, evolve throughout the iterations. The slopes appear to converge to constant values summarised in Table 13, together with the residual correlations. The corresponding probability distributions defined by the sets of values $(\omega, \tau, p)_{m,s}$ from the final iteration are given in Table 16.

Figure 11 illustrates how the maximum normalised misfit, $\max(\varepsilon_{m,s})$, evaluated across all the models m and scenarios s using Equation 12, changes throughout the iterations. The overall tendency is for the maximum misfit to decrease with iterations before converging to the value of around 1.5%. Therefore, the algorithm achives both low misfits between the emulator and the SiBCASA simulations across all the models and scenarios considered, and low levels of the residual inter-scenario bias for each of the three emulator parameters $(\omega, \tau, p)_{m,s}$. This implies that our PCF emulator is robust and its range of applicability can be extended to scenarios such as the 1.5°C and 2°C targets.
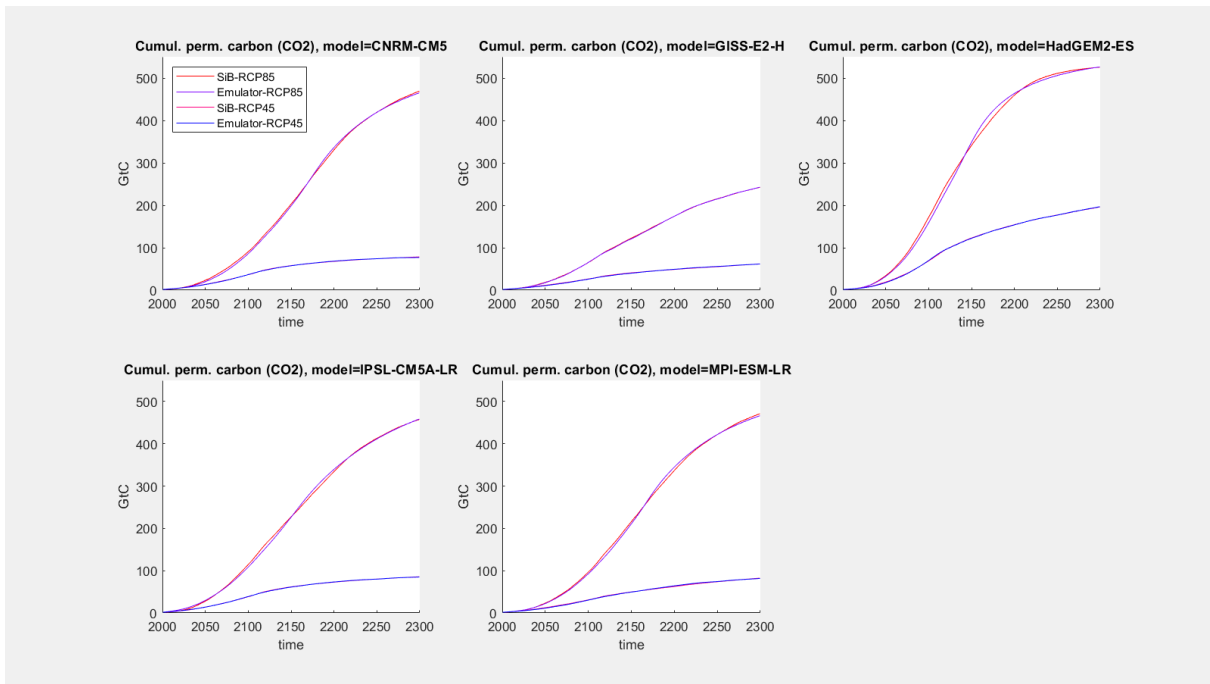

Figure 8. Projections for cumulative land permafrost carbon emissions (CO_2 component) until 2300 under the RCP8.5 and RCP4.5 scenarios, generated by SiBCASA and by our PCF model emulator individually for each of the five CMIP5 models employed in the SiBCASA simulations. In the calibration procedure illustrated by these plots, the emulator was forced by the mean annual GMST projections from the same CMIP5 experiments that were used to conduct the SiBCASA runs. The emulator parameters are from the final iteration. Source: Data_analysis_CO2_SiB_iterations.m.
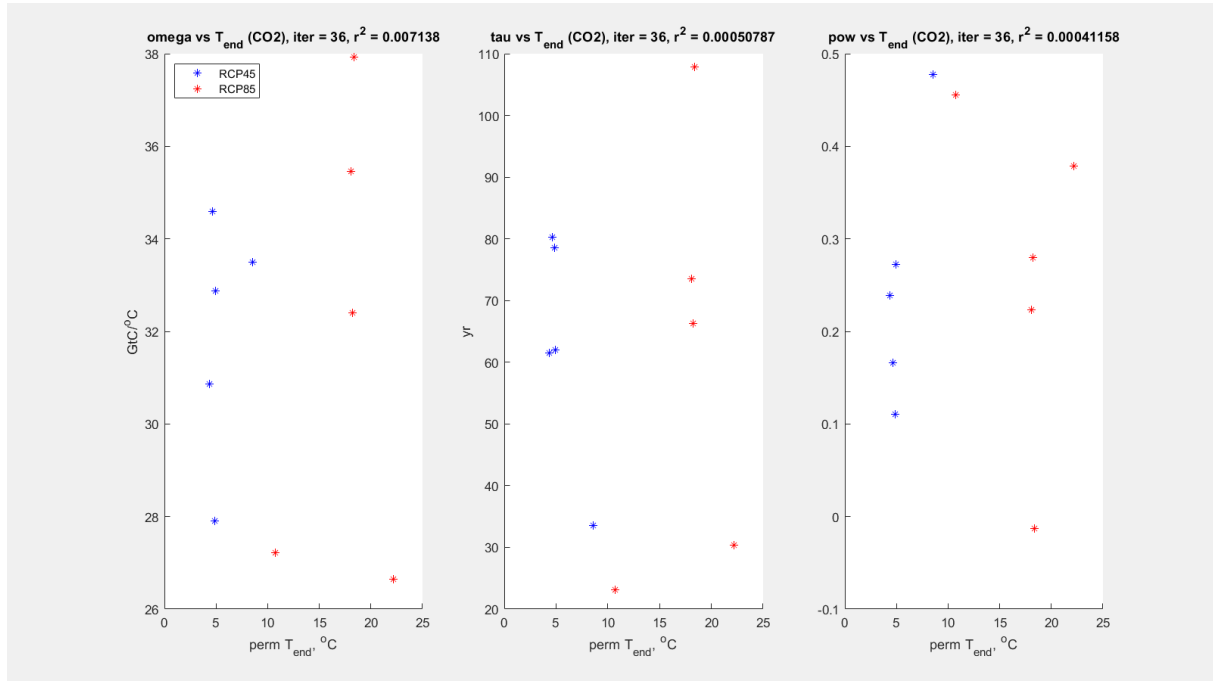
Figure 9. Values of the three emulator parameters $(\omega, \tau, p)_{m,s}$ from the final iteration plotted as functions of the permafrost temperature T_{end} in year 2300 in each SiBCASA run (CO_2 component). The residual inter-scenario biases for the parameters of the dynamic model emulator are described by the correlations that all fall below the required threshold of 0.01. Source: Data_analysis_CO2_SiB_iterations.m.
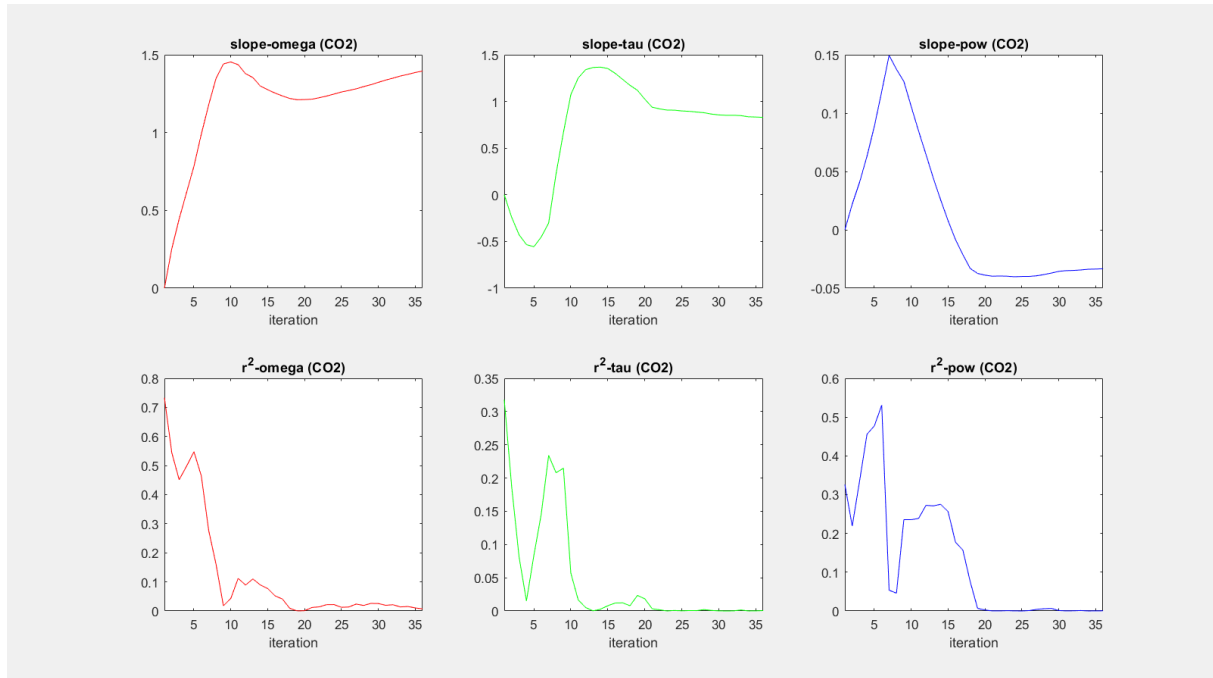

Figure 10. Slopes δ_ω, δ_τ, δ_p defining the corrections to the emulator parameters ω, τ, p in Equation 13 (upper row), and the correlation coefficients $R^2\{\omega_{m,s}, T_{m,s}(t_N)\}, R^2\{\tau_{m,s}, T_{m,s}(t_N)\}, R^2\{p_{m,s}, T_{m,s}(t_N)\}$ (lower row), plotted for all the iterations. SiBCASA, CO_2 component. Source: Data_analysis_CO2_SiB_iterations.m.
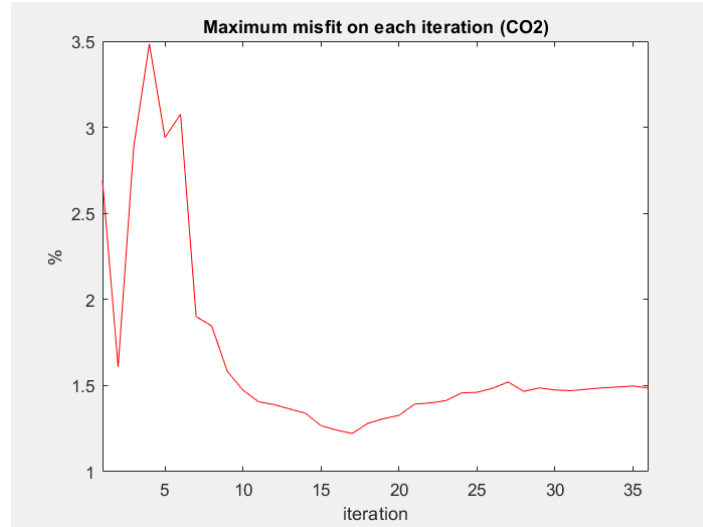
Figure 11. Evolution of the maximum normalised misfit across all the models and scenarios with the iterations. The misfit tends to decrease with the iterations before converging to around 1.5%. SiBCASA, CO_2 component. Source: Data_analysis_CO2_SiB_iterations.m.

Table 13. Results from the final iteration for the slopes δ_ω, δ_τ, δ_p defining the temperature-dependent corrections to ω, τ, p, together with the residual correlations. SiBCASA, CO_2 component. The corresponding probability distributions defined by the sets of values $(\omega, \tau, p)_{m,s}$ from the final iteration are given in Table 16. Source: Data_analysis_CO2_SiB_iterations.m.

Parameter	Value	Units
highest perm temperature, T_{max}	22.2	°C
final iteration number	36	
max_misfit, $\max(\varepsilon_{m,s})\ \forall\ m, s$	0.01486	fraction of 1
slope_omega, δ_ω	1.39535	dimensionless
r2_omega, $R^2\{\omega_{m,s}, T_{m,s}(t_N)\}$	0.00714	fraction of 1
slope_tau, δ_τ	0.82921	dimensionless
r2_tau, $R^2\{\tau_{m,s}, T_{m,s}(t_N)\}$	0.00051	fraction of 1
slope_pow, δ_p	-0.03335	dimensionless
r2_pow, $R^2\{p_{m,s}, T_{m,s}(t_N)\}$	0.00041	fraction of 1

Methane component, SiBCASA

The nonlinear corrections φ_ω, φ_τ, φ_p for the methane component of the PCF emulator of the SiBCASA simulations have a different structure compared with the CO_2 SiBCASA component (Equation 13). The fitting results are presented in the subsequent figures and tables.
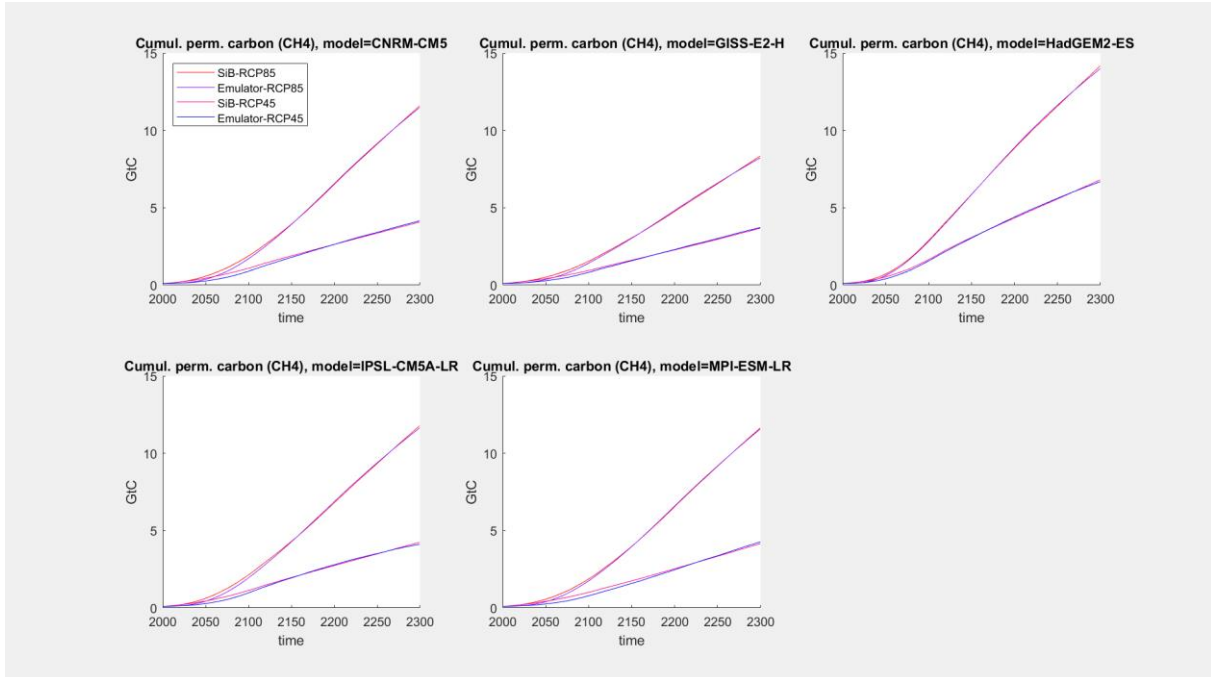
Figure 12. Projections for cumulative land permafrost carbon emissions (methane component) until 2300 under the RCP8.5 and RCP4.5 scenarios, generated by SiBCASA and by our PCF model emulator individually for each of the five CMIP5 models employed in the SiBCASA simulations. In the calibration procedure illustrated by these plots, the emulator was forced by the mean annual GMST projections from the same CMIP5 experiments that were used to conduct the SiBCASA runs. The emulator parameters are from the final iteration. Source: Data_analysis_CH4_SiB_iterations.m.
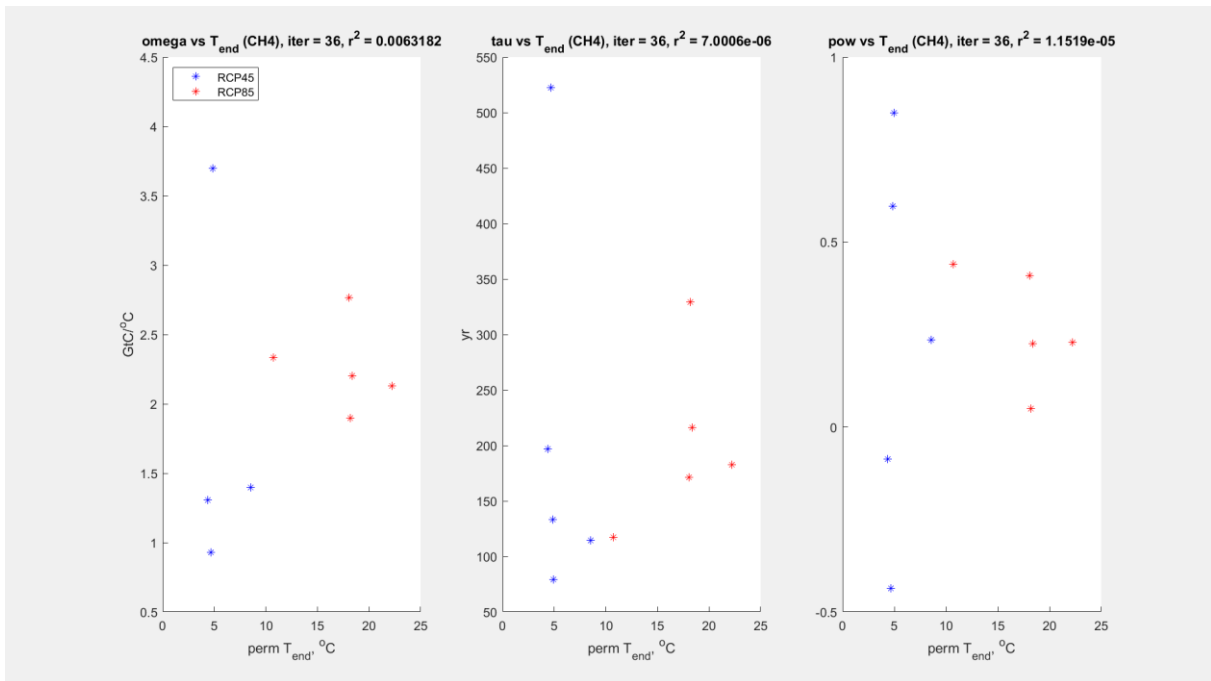
Figure 13. Values of the three emulator parameters $(\omega, \tau, p)_{m,s}$ from the final iteration plotted as functions of the permafrost temperature T_{end} in year 2300 in each SiBCASA run (methane component). The residual inter-scenario biases for the parameters of the dynamic model emulator are described by the correlations that all fall below the required threshold of 0.01. Source: Data_analysis_CH4_SiB_iterations.m.
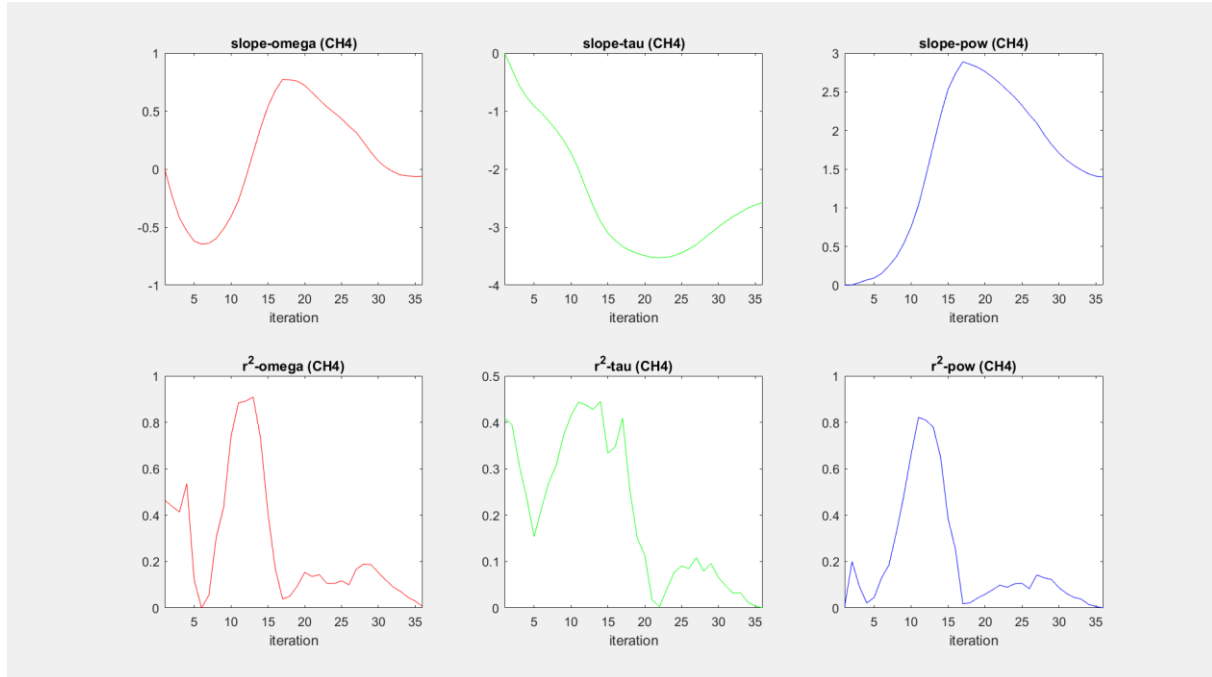
Figure 14. Slopes δ_ω, δ_τ, δ_p defining the corrections to the emulator parameters ω, τ, p in Equation 13 (upper row), and the correlation coefficients $R^2\{\omega_{m,s}, T_{m,s}(t_N)\}, R^2\{\tau_{m,s}, T_{m,s}(t_N)\}, R^2\{p_{m,s}, T_{m,s}(t_N)\}$ (lower row), plotted for all the iterations. SiBCASA, methane component. Source: Data_analysis_CH4_SiB_iterations.m.
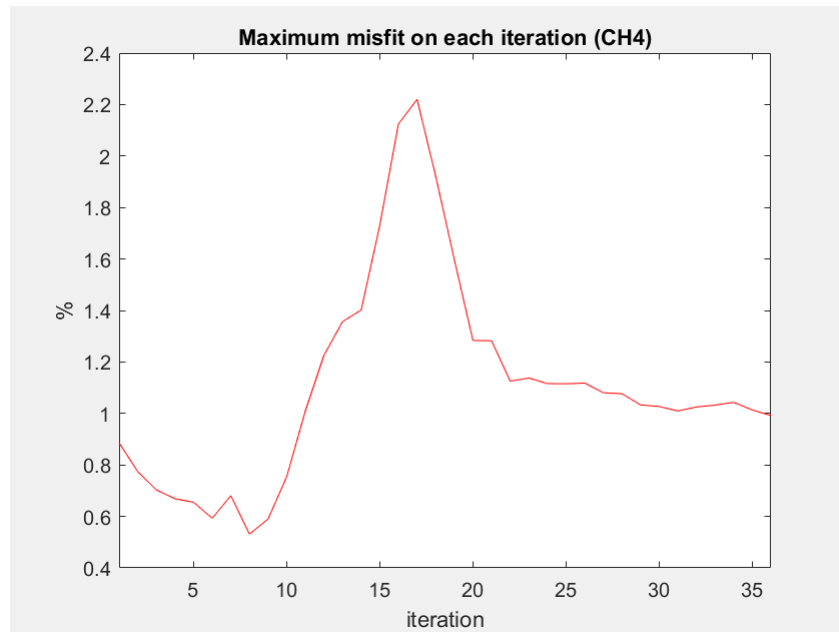

Figure 15. Evolution of the maximum normalised misfit across all the models and scenarios with the iterations. The misfit converges to around 1%. SiBCASA, methane component. Source: Data_analysis_CH4_SiB_iterations.m.

Table 14. Results from the final iteration for the slopes δ_ω, δ_τ, δ_p defining the temperature-dependent corrections to ω, τ, p, together with the residual correlations. SiBCASA, methane component. The corresponding probability distributions defined by the sets of values $(\omega, \tau, p)_{m,s}$ from the final iteration are given in Table 16. Source: Data_analysis_CH4_SiB_iterations.m.

Parameter	Value	Units
highest perm temperature, T_{max}	22.2	°C
final iteration number	36	
max_misfit, $\max(\varepsilon_{m,s})$ $\forall\, m, s$	0.00992	fraction of 1

slope_omega, δ_ω	-0.06163	dimensionless
r2_omega, $R^2\{\omega_{m,s}, T_{m,s}(t_N)\}$	0.00632	fraction of 1
slope_tau, δ_τ	-2.57522	dimensionless
r2_tau, $R^2\{\tau_{m,s}, T_{m,s}(t_N)\}$	0.00001	fraction of 1
slope_pow, δ_p	1.39921	dimensionless
r2_pow, $R^2\{p_{m,s}, T_{m,s}(t_N)\}$	0.00001	fraction of 1

CO2 component, JULES

The emulator of the JULES CO_2 simulations has the same structure as the emulator for the methane component of the SiBCASA simulations (Equation 13), although the resulting numerical values differ. JULES was run with 22 CMIP3 GCMs under 3 emissions scenarios each, giving 66 samples for establishing the statistics in the emulator parameters $(\omega, \tau, p)_{m,s}$. In comparison, SiBCASA was run with only five CMIP5 GCMs under 2 scenarios, giving 10 samples to derive the emulator statistics. The fitting results for the emulator of the JULES CO_2 simulations are presented in the subsequent figures and tables.
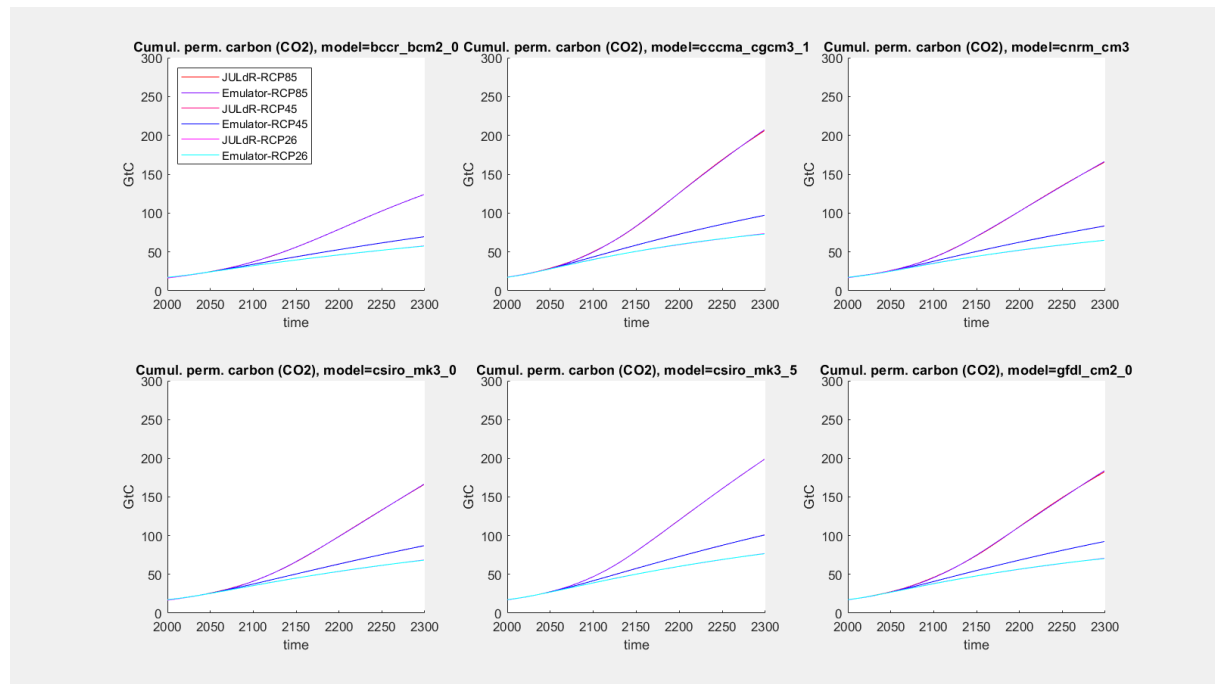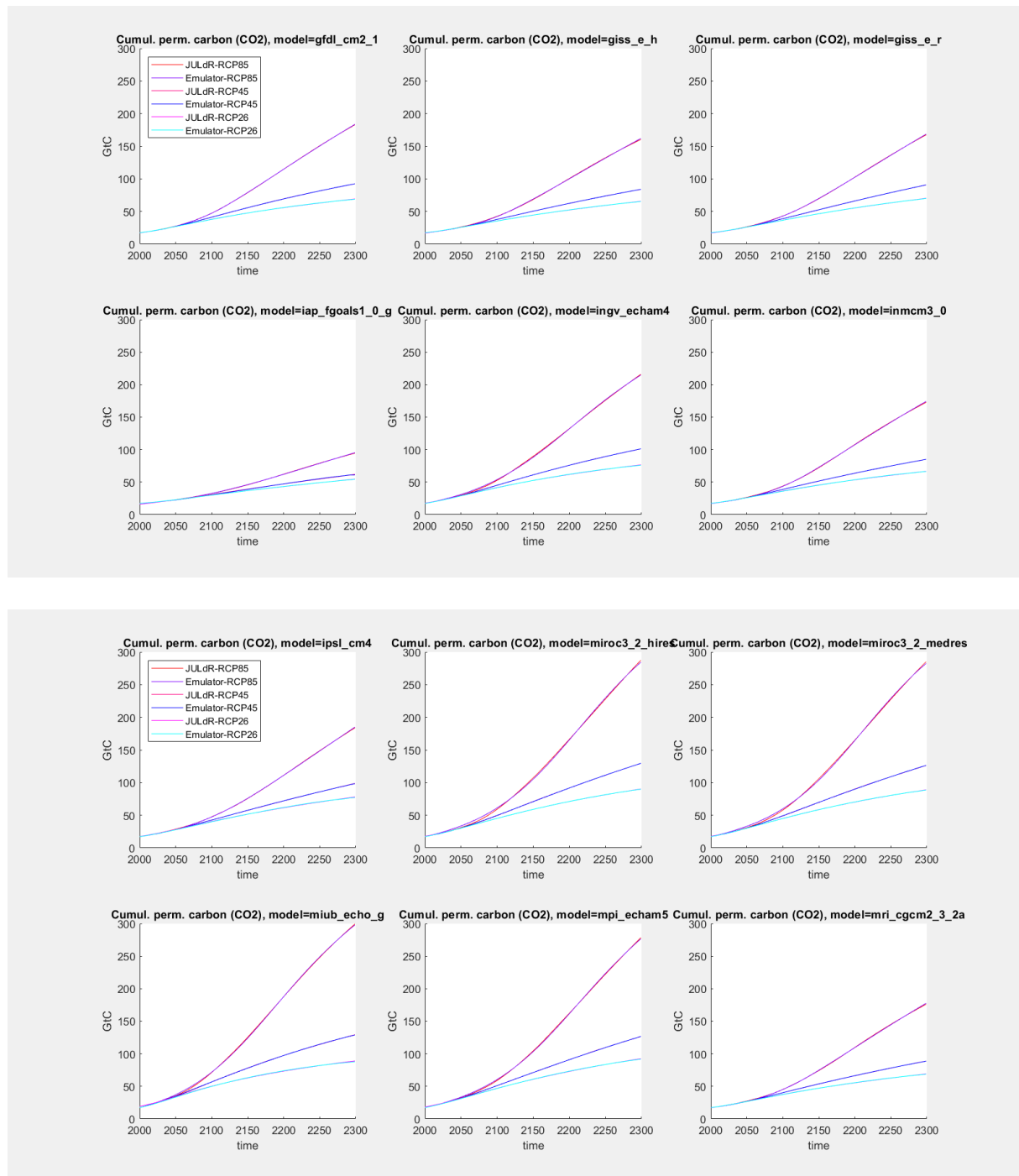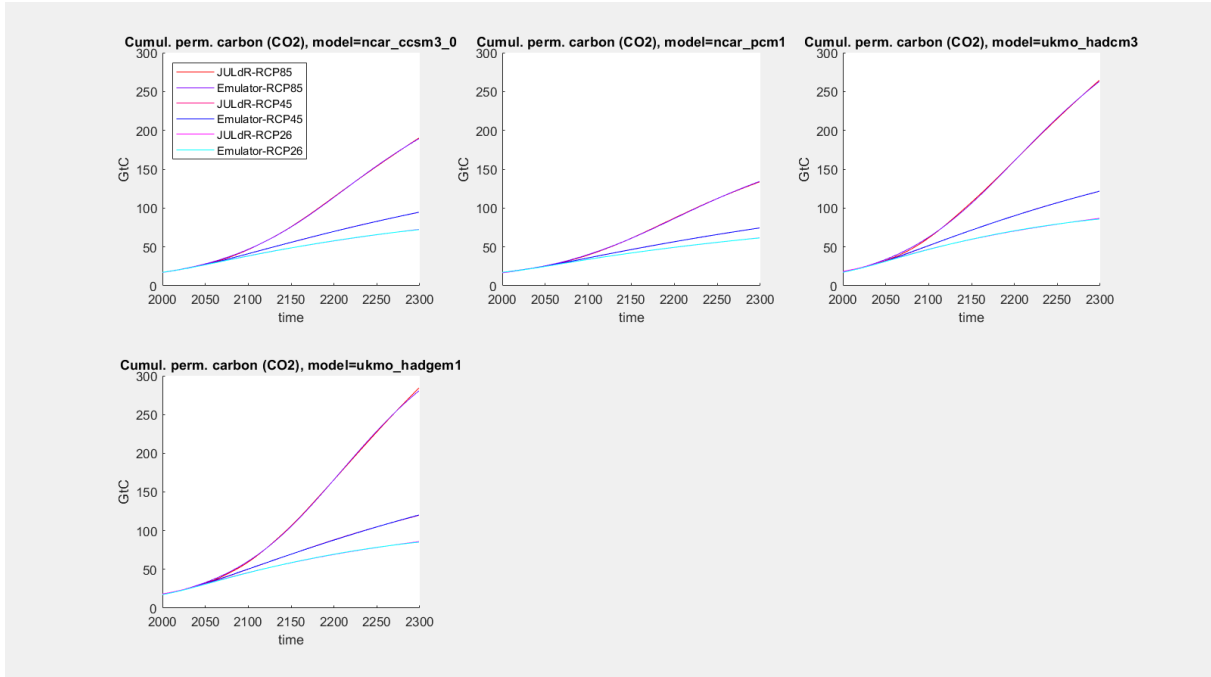
Figure 16. Projections for cumulative land permafrost carbon emissions (CO_2 component) until 2300 under the RCP8.5, RCP4.5 and RCP2.6 scenarios, generated by JULES and by our PCF model emulator individually for each of the 22 CMIP3 models employed in the JULES simulations. In the calibration procedure illustrated by these plots, the emulator was forced by the mean annual GMST projections from the same CMIP3 experiments that were used to conduct the JULES runs. The emulator parameters are from the final iteration. Source: Data_analysis_CO2_JULdR_iterations.m.
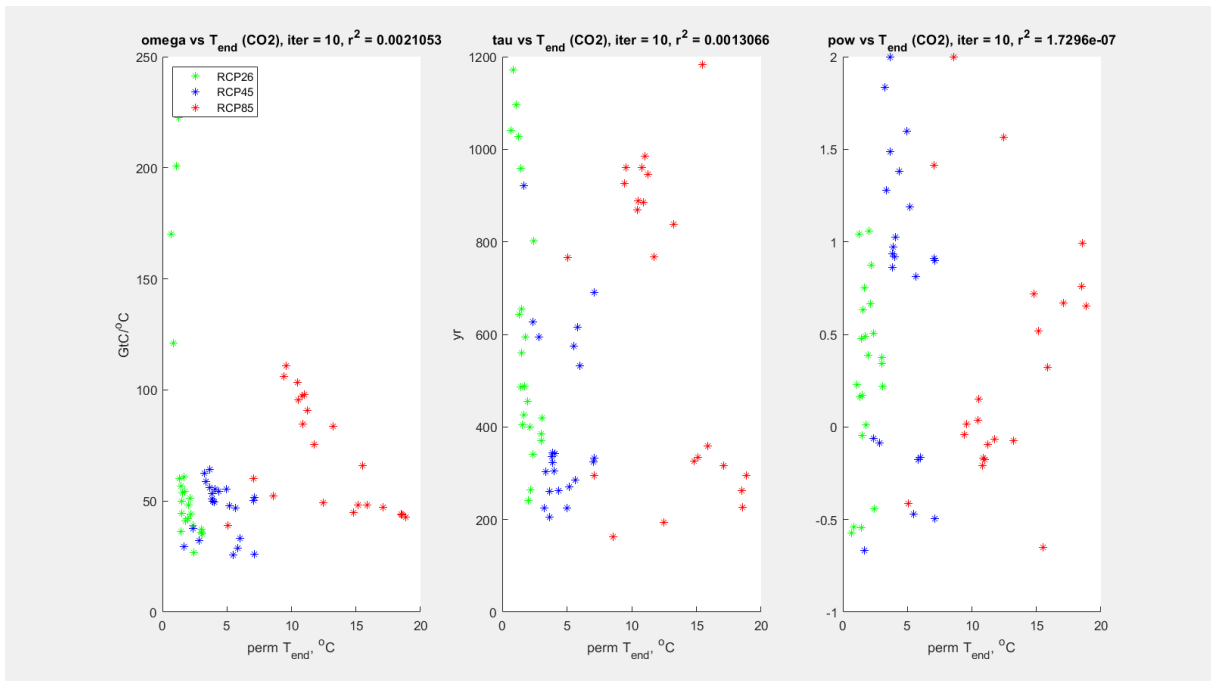

Figure 17. Values of the three emulator parameters $(\omega, \tau, p)_{m,s}$ from the final iteration plotted as functions of the permafrost temperature T_{end} in year 2300 in each JULES run (CO_2 component). The residual inter-scenario biases for the parameters of the dynamic model emulator are described by the correlations that all fall below the required threshold of 0.01. Source: Data_analysis_CO2_JULdR_iterations.m.
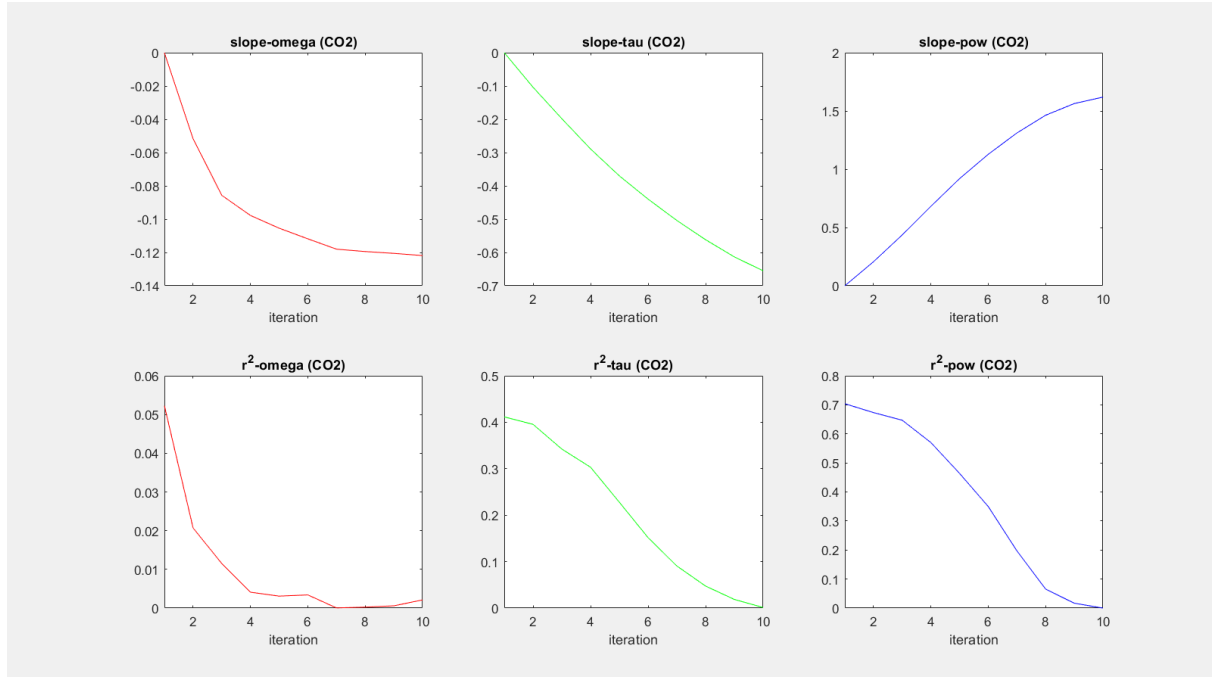
Figure 18. Slopes δ_ω, δ_τ, δ_p defining the corrections to the emulator parameters ω, τ, p in Equation 13 (upper row), and the correlation coefficients $R^2\{\omega_{m,s}, T_{m,s}(t_N)\}, R^2\{\tau_{m,s}, T_{m,s}(t_N)\}, R^2\{p_{m,s}, T_{m,s}(t_N)\}$ (lower row), plotted for all the iterations. JULES, CO_2 component. Source: Data_analysis_CO2_JULdR_iterations.m.
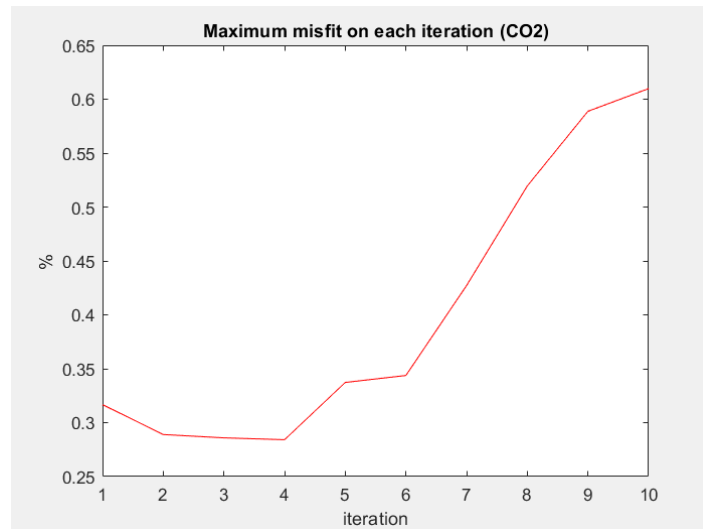

Figure 19. Evolution of the maximum normalised misfit across all the models and scenarios with the iterations. While the misfit increases with the iterations, the increase slows down and the misfit remains at around 0.6% when the required residual inter-scenario bias targets are met for all the three emulator parameters. JULES, CO_2 component. Source: Data_analysis_CO2_JULdR_iterations.m.

Table 15. Results from the final iteration for the slopes δ_ω, δ_τ, δ_p defining the temperature-dependent corrections to ω, τ, p, together with the residual correlations. JULES, CO_2 component. The corresponding probability distributions defined by the sets of values $(\omega, \tau, p)_{m,s}$ from the final iteration are given in Table 16. Source: Data_analysis_CO2_JULdR_iterations.m.

Parameter	Value	Units
highest perm temperature, T_{max}	18.7	°C
final iteration number	10	
max_misfit, $\max(\varepsilon_{m,s}) \ \forall \ m, s$	0.00610	fraction of 1
slope_omega, δ_ω	-0.12187	dimensionless

r2_omega, $R^2\{\omega_{m,s}, T_{m,s}(t_N)\}$	0.00211	fraction of 1
slope_tau, δ_τ	-0.65501	dimensionless
r2_tau, $R^2\{\tau_{m,s}, T_{m,s}(t_N)\}$	0.00131	fraction of 1
slope_pow, δ_p	1.61888	dimensionless
r2_pow, $R^2\{p_{m,s}, T_{m,s}(t_N)\}$	0.00000	fraction of 1

Uncertainty ranges and numerical scheme for the PCF emulator in PAGE-ICE

Table 16 summarises the values of the uncertain parameters defining the PCF emulator, separately for the CO_2 and methane fluxes simulated by SiBCASA. Table 17 replicates the same for the emulator of the CO_2 fluxes simulated by JULES. All the values were obtained using the iterative fitting algorithm described in the sections above. The uncertainty ranges are used to define the associated probability distributions in PAGE-ICE.

The mean equilibrium carbon sensitivity in the CO_2 JULES emulator is around twice larger than in the CO_2 SiBCASA emulator, which in turn is roughly 15 times larger than for the methane SiBCASA emulator. The characteristic time lag in the CO_2 JULES emulator is also the highest, and is nearly 10 times bigger than the lag for the CO_2 SiBCASA emulator. The power parameters determine the nature of convergence to the equilibrium, and they are broadly similar across all the components, albeit with different uncertainty ranges. A combination of these factors implies that the permafrost carbon emissions described by the governing Equation 14 of the emulator are the highest for the CO_2 SiBCASA component. The timing of the emissions also varies greatly between the components, as is illustrated in Figure 8, Figure 12 and Figure 16.

Table 16. Uncertainty ranges for the statistical parameters ω, τ, p defining the PCF emulator in PAGE-ICE, together with the permafrost AF, which are based on the fitting to the SiBCASA simulations with multiple GCMs under multiple climate scenarios. The results are given separately for the CO_2 and methane components. Source: Fitting_results_CO2_SiB_multimod_multiscen_ iterations.xlsx, Fitting_results_CH4_SiB_multimod_multiscen_ iterations.xlsx.

PCF emulator parameters	Min	Mod	Max	Units
AF_p (perm. ampl. factor)	1.43	1.84	2.33	
ω (equilib. sensitivity), CO_2	28,191	31,940	35,688	MtonC/degC
τ (time lag), CO_2	35.49	61.69	87.89	Yr
p (power), CO_2	0.11	0.26	0.41	
ω (equilib. sensitivity), methane	1,240	2,294	3,348	MtonC/degC
τ (time lag), methane	75.19	206.29	337.38	Yr
p (power), methane	-0.11	0.25	0.61	

Table 17. Uncertainty ranges for the statistical parameters ω, τ, p defining the PCF emulator in PAGE-ICE, together with the permafrost AF, which are based on the fitting to the JULES simulations with multiple GCMs under multiple climate scenarios. Source: Fitting_results_CO2_JULdR_multimod_multiscen_ iterations.xlsx

PCF emulator parameters	Min	Mod	Max	Units
AF_p (perm. ampl. factor)	1.71	1.94	2.16	
ω (equilib. sensitivity), CO_2	24,727	61,868	99,009	MtonC/degC

τ (time lag), CO_2	253	544	835	Yr
p (power), CO_2	-0.23	0.46	1.14	

In total, each of the three emulator components (CO_2 SiBCASA, methane SiBCASA, CO_2 JULES) has 4 statistical parameters (Table 16 and Table 17). These are complemented by the 3 slope parameters δ_ω, δ_τ, δ_p defining the nonlinear corrections for the emulator parameters, given in Table 13, Table 14 and Table 15. These parameters are derived by analysing inter-model and inter-scenario datasets and are deterministic as a result.

We solve the governing equation for the cumulative carbon emissions

$$\frac{dC}{dt} = \frac{C_{max}}{\tau\,\varphi_\tau(T)} \cdot \left(\frac{\max\left(C_{eq}(T) - C, 0\right)}{C_{max}}\right)^{(1+p)\,\varphi_p(T)}$$

$$C_{eq}(T) = \min(\omega\,\varphi_\omega(T) \cdot T, C_{max})$$

Equation 14

in closed form on each analysis period $t_{i-1} < t < t_i$, which is possible since the temperature is assumed to be constant during each period. Defining

$$q(T_i) = 1 - (1 + p) \cdot \varphi_p(T_i),$$

the resulting numerical scheme is:

$$C_i = \begin{cases} C_{i-1}, & C_{eq}(T_i) \leq C_{i-1} \\ C_{eq}(T_i), & \left(\dfrac{C_{eq}(T_i) - C_{i-1}}{C_{max}}\right)^{q(T_i)} \leq \dfrac{q(T_i)}{\tau\,\varphi_\tau(T_i)} \cdot (t_i - t_{i-1}) \\ C_{eq}(T_i) - C_{max} \cdot \left[\left(\dfrac{C_{eq}(T_i) - C_{i-1}}{C_{max}}\right)^{q(T_i)} - \dfrac{q(T_i)}{\tau\,\varphi_\tau(T_i)} \cdot (t_i - t_{i-1})\right]^{\frac{1}{q(T_i)}}, & \text{otherwise} \end{cases}$$

Equation 15

Once the permafrost carbon emissions based on SiBCASA and JULES emulators are computed in each analysis year using Equation 15 (either CO_2 or methane components), they are added together with equal weights, and then multiplied by the uncertainty factor for the initial permafrost carbon stock (Hugelius et al., 2014):

$$C(t) = 0.5 \cdot \left(C^{(SiB)}(t) + C^{(JUL)}(t)\right) \cdot (1 + \chi), \quad \chi = 0.01 \cdot \text{Triang}(-15, 0, 15).$$

Equation 16

As JULES does not model permafrost methane emissions explicitly, the latter were inferred from its CO_2 emissions using observational constraints (Schädel et al., 2016):

$$C_{CH4}^{(JUL)} = C_{CO2}^{(JUL)} \cdot \theta, \quad \theta = 0.01 \cdot \text{Triang}(2.8, 6, 9.5).$$

The total cumulative permafrost carbon emissions $C(t)$ from Equation 16 (either CO_2 or methane components) were added to the carbon cycle of the PAGE-ICE model to estimate the effects of the PCF.

Emulator for the nonlinear SAF using CMIP5 simulations

Our nonlinear SAF estimates are based on the ALL/CLR method with atmospheric reflectivity parameterisation (Winton, 2005; Winton, 2006), which uses CMIP5 GCM simulations for atmospheric shortwave radiation fluxes from pre-industrial conditions until either 2100 or 2300 under RCP8.5 scenario. None of the GCM variables were bias-corrected in order to preserve internal consistency of the sea ice and land snow physics in each model. The statistics of the nonlinear SAF assumes model democracy in the CMIP5 sample used (equal weights for all GCMs).

Applying the Winton method to the transient GCM simulations produced time series for the global RF associated with the surface albedo changes. These were differentiated with respect to GMST trends over 30-year climatological windows, separately for each model, using linear polynomial fitting to obtain climatologically-averaged SAF in each year. A Savitzky–Golay filter (base period = 31 years; polynomial order = 1) was applied to obtain smooth time series for GMST and SAF. The SAF (both global total and separately for the three main components) was then represented as a function of the GMST rise individually for each model, at which point the multi model statistics was calculated.

We based the emulator of the global nonlinear SAF (Figure 20) on a two-segment approximation described by the following expressions for the SAF, $f(T)$, and the associated RF, $F(T)$:

$$f(T) = \begin{cases} a_0 + a_1 T + a_2 T^2 + \sigma\varepsilon, & T < T_* \\ b_0 + \rho\varepsilon, & T \geq T_* \end{cases}$$

$$F(T) = \int_0^T f(T')\, dT' = \begin{cases} (a_0 + \sigma\varepsilon)\, T + \dfrac{1}{2} a_1 T^2 + \dfrac{1}{3} a_2 T^3, & T < T_* \\ (a_0 + \sigma\varepsilon)\, T_* + \dfrac{1}{2} a_1 T_*^2 + \dfrac{1}{3} a_2 T_*^3 + (b_0 + \rho\varepsilon)\cdot(T - T_*), & T \geq T_* \end{cases}$$
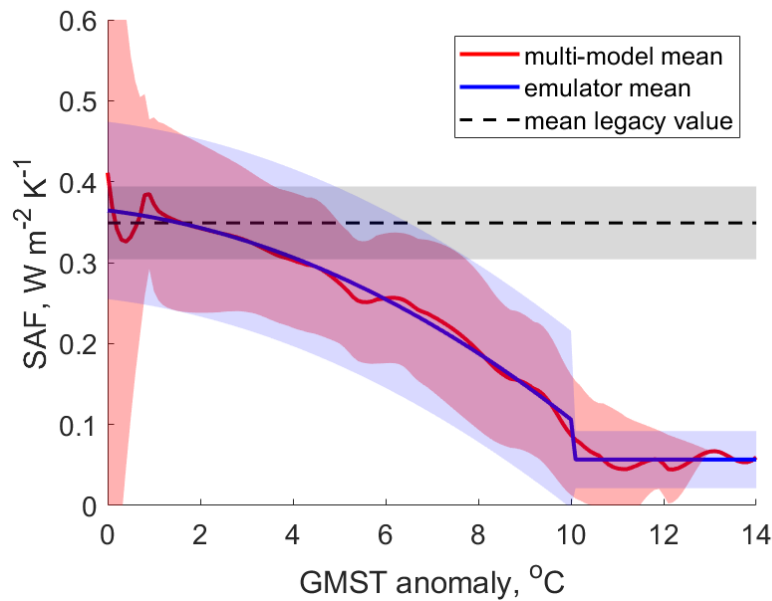
Equation 17

Figure 20. Global SAF as a function of the GMST rise relative to pre-industrial conditions obtained from multiple CMIP5 GCMs using Winton's method. Red line: multi-model mean; shaded red area: ±1 SD; blue line and shaded area: mean and ±1 SD of the two-segment emulator. The dashed line and grey shaded area show statistical mean and ±1 SD of the SAF averaged between pre-industrial conditions and the level of warming corresponding to the 2xCO₂ ECS experiment (mean value of 2.8°C, 5-95% range of 1.7°C to 4.2°C according to IPCC AR5). Source: Yumashev et al. (2019).

Here T is the GMST anomaly, $T_* = 10°C$ is the empirically determined switch between the quadratic and constant SAF segments (Figure 20), a_j are the coefficients of quadratic polynomial fitting to the multi-model mean global SAF over the $T < T_*$ segment, b_0 is average of the multi-model mean global SAF over the $T \geq T_*$ segment, $\sigma(\rho)$ is average of the multi-model SD of the global SAF over the $T < T_*$ ($T \geq T_*$) segment, and $\varepsilon = \mathcal{N}(0,1)$.

Details of the CMIP5 models used for the SAF emulator

We computed the SAF from 16 CMIP5 models that have the necessary variables to apply Winton's ALL/CLR method: rsus, rsds, rsdscs and rsdt (Winton, 2005). A complete list of these models can be found in Table 18. The following eight models provided the variables until 2300: BCC-CSM1.1, CCSM4, CNRM-CM5, CSIRO-Mk3.6.0, GISS-E2-H, HadGEM2-ES, IPSL-CM5A-LR and MPI-ESM-LR. The other eight models provided the data until 2100. Each model has its own domains for Arctic sea-ice (sic) and land snow (snc) covers based on their respective monthly maximum extents during the pre-industrial period (1850-1900), with the exception of the model IPSL-CM5A-LR, which only allowed the computation of a northern hemispheric sea-ice domain. We did not apply bias-correcting to the sea ice, land snow and GMST simulations to preserve the internal consistency in the physics for each model.

*Table 18. CMIP5 model simulations used for computing the SAF based on Winton's method. The models marked with **(P)** were also used to drive SiBCASA LSM simulations to calculate the PCF.*

Modeling Center (or Group)	Institute ID	Model Name

Commonwealth Scientific and Industrial Research Organization (CSIRO) and Bureau of Meteorology (BOM), Australia	CSIRO-BOM	ACCESS1.3
Beijing Climate Center, China Meteorological Administration	BCC	BCC-CSM1.1
Canadian Centre for Climate Modelling and Analysis	CCCMA	CanESM2
National Center for Atmospheric Research	NCAR	CCSM4
Community Earth System Model Contributors	NSF-DOE-NCAR	CESM1(CAM5)
Centre National de Recherches Météorologiques / Centre Européen de Recherche et Formation Avancée en Calcul Scientifique	CNRM-CERFACS	CNRM-CM5 **(P)**
Commonwealth Scientific and Industrial Research Organization in collaboration with Queensland Climate Change Centre of Excellence	CSIRO-QCCCE	CSIRO-Mk3.6.0
NOAA Geophysical Fluid Dnamics Laboratory	NOAA GFDL	GFDL-CM3
NASA Goddard Institute for Space Studies	NASA GISS	GISS-E2-H **(P)**
Met Office Hadley Centre (additional HadGEM2-ES realizations contributed by Instituto Nacional de Pesquisas Espaciais)	MOHC (additional realizations by INPE)	HadGEM2-ES **(P)**
Institute for Numerical Mathematics	INM	INM-CM4
Institut Pierre-Simon Laplace	IPSL	IPSL-CM5A-LR **(P)**
Japan Agency for Marine-Earth Science and Technology, Atmosphere and Ocean Research Institute (The University of Tokyo), and National Institute for Environmental Studies	MIROC	MIROC-ESM
Max-Planck-Institut für Meteorologie (Max Planck Institute for Meteorology)	MPI-M	MPI-ESM-LR **(P)**
Meteorological Research Institute	MRI	MRI-CGCM3
Norwegian Climate Centre	NCC	NorESM1-ME

Implementation of the SAF emulator in PAGE-ICE

The emulator recognises that the SAF is implicitly included in the $2xCO_2$ equilibrium climate sensitivity parameter (ECS), which is central to modelling the greenhouse effect in IAMs like

PAGE, DICE and FUND.[23] Without acknowledging the baseline level of the SAF used in the ECS parameter, which we refer to as the legacy value, simply adding it to the anthropogenic RF would amount to double-counting. To date, none of the IAMs have had a temperature-varying ECS to reflect the nonlinear (state-dependent) nature of planetary feedbacks such as the SAF. The $2xCO_2$ ECS parameter in PAGE-ICE is consistent with the range in IPCC AR5, which is based on paleo-records, CMIP5 simulations and $2xCO_2$ experiments in climate emulators of intermediate complexity. The corresponding mean equilibrium warming is 2.8°C (5-95% range of 1.7°C to 4.2°C). According to the GCMs' simulations analysed, the statistical mean value of the average level of the global SAF for the period between pre-industrial conditions and the $2xCO_2$ ECS warming is $f^{(ecs)} = 0.349 \pm 0.045$ W/m²/K, which is in good agreement with historic data (Flanner et al., 2011; Pistone et al., 2014; Cao et al., 2015). The implicit baseline assumption in IAMs to date has been that of a constant legacy SAF equal to $f^{(ecs)}$. This is equivalent to the RF due to the surface albedo changes extrapolated linearly with the GMST anomaly T relative to the pre-industrial conditions (1850-1900):

$$F^{(ecs)}(T) = f^{(ecs)} \cdot T.$$

Equation 18

To capture the effect of the state-dependent SAF under future climate scenarios, we used the nonlinear emulator (Methods) and evaluated it in the analysis years t_i of PAGE-ICE. We employed piece-wise linear interpolation with respect to GMST for each analysis period $t_{i-1} < t < t_i$ characterized by the temperature range $T_{i-1} < T < T_i$, resulting the following SAF-driven increase in the RF relative to the pre-industrial (1850-1900) conditions:

$$F^{(int)}(T) = F(T_{i-1}) + f_{i-1}^{(int)} \cdot (T - T_{i-1}), \quad f_{i-1}^{(int)} = \frac{F(\hat{T}_i) - F(T_{i-1})}{\hat{T}_i - T_{i-1}}.$$

Equation 19

Here $\hat{T}_i$ is a preliminary temperature estimate in year t_i before the nonlinear SAF correction is introduced (that is, based on the legacy SAF value introduced above), $F(T)$ is the probabilistic RF from the SAF emulator which is given in the Methods section of the main article and Equation 2 therein, $f_{i-1}^{(int)}$ is the resulting constant SAF approximation over the analysis period $t_{i-1} < t < t_i$, and $F^{(int)}(T)$ is the corresponding linearly interpolated RF for the same analysis period.

The difference between the nonlinear RF (Equation 19, interpolated over a given analysis period) and linearly extrapolated cumulative RF (Equation 18, corresponding to the constant legacy SAF) during the analysis period $t_{i-1} < t < t_i$ is

$$\Delta F^{(corr)}(T) = F^{(int)}(T) - F^{(ecs)}(T) = \left(F(T_{i-1}) - f_{i-1}^{(int)} \cdot T_{i-1} \right) + \left(f_{i-1}^{(int)} - f^{(ecs)} \right) \cdot T$$
$$\equiv \Delta F_{i-1}^{(corr)} + \Delta f_{i-1}^{(corr)} \cdot T, \qquad T_{i-1} < T < T_i$$

where we defined

---

[23] Unlike the CMIP5 definition of the ECS, which is based on the abrupt $4xCO_2$ experiment, PAGE-ICE employs the more generic IPCC AR5 definition based on the $2xCO_2$ increase relative to pre-industrial conditions.

$$\Delta F_{i-1}^{(corr)} = F(T_{i-1}) - f_{i-1}^{(int)} \cdot T_{i-1}, \qquad \Delta f_{i-1}^{(corr)} = \left(f_{i-1}^{(int)} - f^{(ecs)} \right).$$

As a result, the nonlinear correction to the SAF alters the governing equation for the GMST change in PAGE-ICE by adding extra terms to the total anthropogenic RF, $F^{(ant)}(t)$, which modifies the 2xCO₂ equilibrium climate sensitivity parameter ECS (°C) and the e-folding feedback response time FRT (yr) of the upper ocean layers to increased RF. For the analysis period $t_{i-1} < t < t_i$, the GMST equation becomes:

$$\frac{dT}{dt} = \frac{1}{\text{FRT}_{i-1}^{(corr)}} \cdot \left[\frac{\text{ECS}_{i-1}^{(corr)}}{F_{sl} \ln 2} \cdot \left(F^{(ant)}(t) + \Delta F_{i-1}^{(corr)} \right) - T \right].$$

Equation 20

Here

$$\text{ECS}_{i-1}^{(corr)} = \text{ECS} \cdot \left[1 - \frac{\text{ECS}}{F_{sl} \ln 2} \Delta f_{i-1}^{(corr)} \right]^{-1}, \qquad \text{FRT}_{i-1}^{(corr)} = \text{FRT} \cdot \left[1 - \frac{\text{ECS}}{F_{sl} \ln 2} \Delta f_{i-1}^{(corr)} \right]^{-1}$$

are the modified ECS and FRT parameters adjusted in each analysis year according to the change $\Delta f_{i-1}^{(corr)}$ in the SAF relative to the constant legacy value; F_{sl} (W/m²) is the RF slope parameter for the logarithmic CO₂ RF law. This is a standard exponential lagged model for the greenhouse effect.
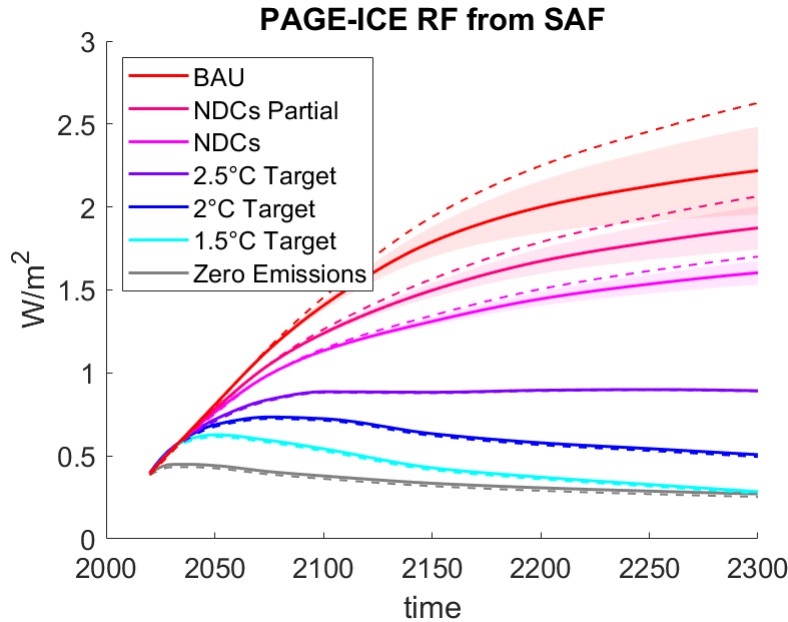

Figure 21. Global equivalent RF from the nonlinear SAF (solid lines: mean; shaded areas: ±1 SD) and cumulative RF corresponding to temperature-invariant SAF of 0.349±0.045 W/m2/°C, which represents average SAF for the period between pre-industrial conditions and the 2xCO2 ECS warming level (dashed lines), plotted for the climate scenarios considered. 100,000 Monte-Carlo runs of PAGE-ICE. Source: Yumashev et al. (2019).

Equation 20 was solved in closed form during each analysis period $t_{i-1} < t < t_i$, which is possible since the temperature is assumed to be constant during each period, using an improved technique described in the sections on the GMTS calculations in PAGE-ICE above.

The resulting difference between the cumulative RF from the nonlinear SAF and constant legacy SAF is plotted in Figure 21 for the climate scenarios considered. The nonlinear SAF is marginally higher than the legacy SAF for the lower emissions scenarios, before dropping below the legacy SAF as the Arctic sea ice and land snow covers disappear. As a result, the RF based on the nonlinear SAF is lower than the RF from the constant legacy SAF for the higher emissions scenarios; this effect is particularly strong for BAU in the 23rd century. This implies that the IAMs such as PAGE, DICE and FUND slightly underestimated the effect of the nonlinear SAF for the low emissions scenarios, and overestimated it for the medium and high emissions scenarios.

Complete list of the CMIP5 and CMIP3 models used in the study

*Table 19. List of CMIP5 GCMs used in different parts of the study. The selected models that were used to calibrate the PCF and SAF are marked as **(P)** and **(S)**, respectively.*

Modeling Center (or Group)	Institute ID	Model Name
Commonwealth Scientific and Industrial Research Organization in collaboration with Bureau of Meteorology	CSIRO-BOM	ACCESS1.0 ACCESS1.3 **(S)**
Beijing Climate Center, China Meteorological Administration	BCC	BCC-CSM1.1 **(S)** BCC-CSM1.1-m
Beijing Normal University	BNU	BNU-GCM
Canadian Centre for Climate Modelling and Analysis	CCCMA	CanESM2 **(S)**
National Center for Atmospheric Research	NCAR	CCSM4 **(S)**
Community Earth System Model Contributors	NSF-DOE-NCAR	CESM1-BGC CESM1-CAM5 **(S)**
Centro Euro-Mediterraneo sui Cambiamenti Climatici	CMCC	CMCC-CESM CMCC-CM CMCC-CMS
Centre National de Recherches Météorologiques / Centre Européen de Recherche et Formation Avancée en Calcul Scientifique	CNRM-CERFACS	CNRM-CM5 **(P, S)**
Commonwealth Scientific and Industrial Research Organization in collaboration with Queensland Climate Change Centre of Excellence	CSIRO-QCCCE	CSIRO-Mk3.6.0 **(S)**
EC-EARTH consortium	EC-EARTH	EC-EARTH
LASG, Institute of Atmospheric Physics, Chinese Academy of Sciences and CESS, Tsinghua University	LASG-CESS	FGOALS-g2

LASG, Institute of Atmospheric Physics, Chinese Academy of Sciences	LASG-IAP	FGOALS-s2
Geophysical Fluid Dynamics Laboratory	GFDL	GFDL-CM3 **(S)**
NASA Goddard Institute for Space Studies	NASA GISS	GISS-E2-H **(P, S)** GISS-E2-H-CC GISS-E2-R GISS-E2-R-CC
Met Office Hadley Centre (additional HadGEM2-ES realizations contributed by Instituto Nacional de Pesquisas Espaciais)	MOHC	HadGEM2-ES **(P, S)**
Institute for Numerical Mathematics	INM	INM-CM4 **(S)**
Institut Pierre-Simon Laplace	IPSL	IPSL-CM5A-LR **(P, S)** IPSL-CM5A-MR IPSL-CM5B-LR
Japan Agency for Marine-Earth Science and Technology, Atmosphere and Ocean Research Institute (The University of Tokyo), and National Institute for Environmental Studies	MIROC	MIROC-GCM **(S)** MIROC-GCM-CHEM
Atmosphere and Ocean Research Institute (The University of Tokyo), National Institute for Environmental Studies, and Japan Agency for Marine-Earth Science and Technology	MIROC	MIROC5
Max-Planck-Institut für Meteorologie (Max Planck Institute for Meteorology)	MPI-M	MPI-GCM-MR MPI-ESM-LR **(P, S)**
Meteorological Research Institute	MRI	MRI-CGCM3 **(S)**
Norwegian Climate Centre	NCC	NorESM1-M NorESM1-ME **(S)**

Table 20. List of CMIP3 GCMs that were used with the JULES LSM to simulate permafrost carbon emissions.

Modeling Center (or Group)	Institute ID	Model Name
Beijing Climate Center, China Meteorological Administration	BCC	bccr_bcm2_0
Canadian Centre for Climate Modelling and Analysis	CCCMA	cccma_cgcm3_1
Centre National de Recherches Météorologiques	CNRM	cnrm_cm3
Commonwealth Scientific and Industrial Research Organization	CSIRO	csiro_mk3_0 csiro_mk3_5
Geophysical Fluid Dynamics Laboratory	GFDL	gfdl_cm2_0 gfdl_cm2_1

NASA Goddard Institute for Space Studies	NASA GISS	giss_e_h giss_e_r
LASG, Institute of Atmospheric Physics, Chinese Academy of Sciences	LASG-IAP	iap_fgoals1_0_g
European Topic Centre on Climate Change	INGV	ingv_echam4
Institute for Numerical Mathematics	INM	inmcm3_0
Institut Pierre-Simon Laplace	IPSL	ipsl_cm4
Japan Agency for Marine-Earth Science and Technology, Atmosphere and Ocean Research Institute (The University of Tokyo)	MIROC	miroc3_2_hires miroc3_2_medres
Meteorological Institute of the University of Bonn	MIUB	miub_echo_g
Max-Planck-Institut für Meteorologie (Max Planck Institute for Meteorology)	MPI-M	mpi_echam5
Meteorological Research Institute	MRI	mri_cgcm2_3_2a
National Center for Atmospheric Research	NCAR	ncar_ccsm3_0 ncar_pcm1
Met Office Hadley Centre	MOHC	ukmo_hadcm3 ukmo_hadgem1

Acknowledgements

References

Yumashev, D., Hope, C., Schaefer, K., Riemann-Campe, K., Iglesias-Suarez, F., Jafarov, E., Burke, E.J., Young, P.J., Elshorbany, Y., Whiteman, G. Climate policy implications of nonlinear decline of Arctic land permafrost, snow and sea ice. *Nature Communications*, 10, Article number: 1900. DOI 10.1038/s41467-019-09863-x. 2019

Hope, C. The marginal impact of CO2 from PAGE2002: An integrated assessment model incorporating the IPCC's five reasons for concern. *Integrated assessment*, 6(1). 2006.

Hope, C. Critical issues for the calculation of the social cost of CO2: why the estimates from PAGE09 are higher than those from PAGE2002. *Climatic Change*, 117(3), 531-543. 2013.

Riahi, K., Van Vuuren, D. P., Kriegler, E., Edmonds, J., O'neill, B. C., Fujimori, S., ... & Lutz, W. The shared socioeconomic pathways and their energy, land use, and greenhouse gas emissions implications: an overview. *Global Environmental Change*, 42, 153-168. 2017.

Joos, F., Roth, R., Fuglestvedt, J. S., Peters, G. P., ... & Friedrich, T. Carbon dioxide and climate impulse response functions for the computation of greenhouse gas metrics: a multi-model analysis. *Atmospheric Chemistry and Physics*, 13(5), 2793-2825. 2013.

Shindell, D., & Faluvegi, G. Climate response to regional radiative forcing during the twentieth century. *Nature Geoscience*, *2*(4), 294. 2009.

Nauels, A., Rogelj, J., Schleussner, C. F., Meinshausen, M., & Mengel, M. Linking sea level rise and socioeconomic indicators under the Shared Socioeconomic Pathways. *Environmental Research Letters*, 12(11), 114002. 2017.

Golledge, N. R., Kowalewski, D. E., Naish, T. R., Levy, R. H., Fogwill, C. J., & Gasson, E. G. The multi-millennial Antarctic commitment to future sea-level rise. *Nature*, 526(7573), 421-425. 2015.

Hansen, J., Sato, M., Hearty, P., Ruedy, R., Kelley, ... & Velicogna, I. Ice melt, sea level rise and superstorms: evidence from paleoclimate data, climate modeling, and modern observations that 2 C global warming could be dangerous. *Atmospheric Chemistry and Physics,* 16(6), 3761-3812. 2016.

Le Bars, D., Drijfhout, S., and de Vries, H. A high-end sea level rise probabilistic projection including rapid Antarctic ice sheet mass loss. *Environmental Research Letters*, *12*(4), 044013. 2017.

Burke, M., Hsiang, S. M., & Miguel, E. Global non-linear effect of temperature on economic production. *Nature*, 527(7577), 235-239. 2015.

Christensen, P., Gillingham, K., & Nordhaus, W. Uncertainty in forecasts of long-run economic growth. *Proceedings of the National Academy of Sciences*, 115(21), 5409-5414. 2018.

Aldy, J., Pizer, W., Tavoni, M., Reis, L. A., Akimoto, K., Blanford, G., ... & McJeon, H. C. Economic tools to promote transparency and comparability in the Paris Agreement. *Nature Climate Change*, 6(11), 1000-1004. 2016.

Rubin, E. S., Azevedo, I. M., Jaramillo, P., & Yeh, S. A review of learning rates for electricity supply technologies. *Energy Policy*, 86, 198-218. 2015.

International Energy Agency (IEA) Energy technology perspectives 2012 – Pathways to a clean energy system. Paris, France. 2012.

Anthoff, D., Hepburn, C. and Tol. R.S.J. Equity weighting and the marginal damage costs of climate change, *Ecological Economics*, Volume 68, Issue 3, 836-849. 2009.

Taylor, K. E., Stouffer, R. J., & Meehl, G. A. An overview of CMIP5 and the experiment design. *Bulletin of the American Meteorological Society*, *93*(4), 485-498. 2012.

Van Vuuren, D. P., Edmonds, J., Kainuma, M., Riahi, K., Thomson, A., Hibbard, K., ... & Masui, T. The representative concentration pathways: an overview. *Climatic Change*, 109(1-2), 5. 2011.

Keenan, T. F., Prentice, I. C., Canadell, J. G., Williams, C. A., Wang, H., Raupach, M., & Collatz, G. J. Recent pause in the growth rate of atmospheric CO2 due to enhanced terrestrial carbon uptake. *Nature Communications*, 7, 13428. 2016.

Fernández-Martínez, M., Sardans, J., Chevallier, F., Ciais, P., Obersteiner, M., Vicca, S., ... & Piao, S. L. Global trends in carbon sinks and their relationships with CO 2 and temperature. *Nature Climate Change*. 2018.

Omta, A. W., Dutkiewicz, S., & Follows, M. J. Dependence of the ocean-atmosphere partitioning of carbon on temperature and alkalinity. *Global Biogeochemical Cycles*, 25(1). 2011.

Eyring, V., Arblaster, J. M., Cionni, I., Sedláček, J., Perlwitz, J., Young, P. J., ... & Faluvegi, G. Long-term ozone changes and associated climate impacts in CMIP5 simulations. *Journal of Geophysical Research: Atmospheres*, 118(10), 5029-5060. 2013.

Alexeev, V. A., Langen, P. L., & Bates, J. R. Polar amplification of surface warming on an aquaplanet in "ghost forcing" experiments without sea ice feedbacks. *Climate Dynamics*, 24(7-8), 655-666. 2015.

Grinsted, A., Moore, J. C., & Jevrejeva, S. Reconstructing sea level from paleo and projected temperatures 200 to 2100 AD. *Climate Dynamics*, 34(4), 461-472. 2009.

Knutti, R., & Sedláček, J. Robustness and uncertainties in the new CMIP5 climate model projections. *Nature Climate Change*, 3(4), 369. 2013.

McKinsey & Company. Abatement Cost Curve; International Energy Agency World Energy Outlook, US Environmental Protection Agency. European Environment Agency (EEA). 2009.

Piontek, F., Kalkuhl, M., Kriegler, E., Schultes, A., Leimbach, M., Edenhofer, O., & Bauer, N. Economic Growth Effects of Alternative Climate Change Impact Channels in Economic Modeling. *Environmental and Resource Economics*, 1-29. 2018.

Schaefer, K., T. Zhang, L. Bruhwiler, and A. P. Barrett. Amount and timing of permafrost carbon release in response to climate warming, Tellus Series B: *Chemical and Physical Meteorology*, 63(2), pg. 165-180. 2011.

Burke, E. J., Ekici, A., Huang, Y., Chadburn, S. E., Huntingford, C., Ciais, P., ... & Krinner, G. Quantifying uncertainties of permafrost carbon–climate feedbacks. *Biogeosciences*, 14(12), 3051. 2017.

Schaefer, K., Zhang, T., Slater, A. G., Lu, L., Etringer, A. and Baker, I. Improving simulated soil temperatures and soil freeze/thaw at high-latitude regions in the Simple Biosphere/Carnegie-Ames-Stanford Approach model. *J. Geophys. Res.*, 114, art. num F02021. 2009.

Schaefer, K; and E. Jafarov. A parameterization of respiration in frozen soils based on substrate availability. *Biogeosciences*, 13, 1991–2001. 2016.

Jafarov, E. and Schaefer, K.: The importance of a surface organic layer in simulating permafrost thermal and carbon dynamics, *The Cryosphere*, 10, 465-475. 2016.

Hugelius, G., Tarnocai, C., Broll, G., Canadell, J. G., Kuhry, P., and Swanson, D. K. The Northern Circumpolar Soil Carbon Database: spatially distributed datasets of soil coverage and soil carbon storage in the northern permafrost regions, *Earth Syst. Sci. Data*, 5, 3–13. 2013.

Wei, Y, Liu, S, Huntzinger, DN, Michalak, AM, …, Shi, X. The North American Carbon Program Multi-scale Synthesis and Terrestrial Model Intercomparison Project - Part 2: Environmental driver data, *Geosci. Model Devel.*, (7)6, 2875-2893. 2014

Chadburn, S., Burke, E., Essery, R., Boike, J., Langer, M., Heikenfeld, M., ... & Friedlingstein, P. An improved representation of physical permafrost dynamics in the JULES land-surface model. *Geoscientific Model Development*, 8(5), 1493-1508. 2015.

Burke, E. J., Chadburn, S. E., & Ekici, A. A vertical representation of soil carbon in the JULES land surface scheme (vn4. 3_permafrost) with a focus on permafrost regions. *Geoscientific Model Development*, 10(2), 959-975. 2017b.

Zimov, S. A., Schuur, E. A., & Chapin, F. S. Permafrost and the global carbon budget. *Science*, 312(5780), 1612-1613. 2006.

Mengel, M., Nauels, A., Rogelj, J., & Schleussner, C. F. Committed sea-level rise under the Paris Agreement and the legacy of delayed mitigation action. *Nature Communications*, 9(1), 601. 2018.

Schädel, C., Bader, M. K. F., Schuur, E. A., Biasi, C., Bracho, R., Čapek, P., ... & Graham, D. E. Potential carbon emissions dominated by carbon dioxide from thawed permafrost soils. *Nature Climate Change*, 6(10), 950. 2016.

Winton, M. Simple optical models for diagnosing surface–atmosphere shortwave interactions. *Journal of Climate*, 18(18), 3796-3805. 2005

Winton, M. Surface albedo feedback estimates for the AR4 climate models. *Journal of Climate*, 19(3), 359-365. 2006

Flanner, M. G., Shell, K. M., Barlage, M., Perovich, D. K., & Tschudi, M. A. Radiative forcing and albedo feedback from the Northern Hemisphere cryosphere between 1979 and 2008. *Nature Geoscience*, 4(3), 151. 2011.

Pistone, K., Eisenman, I., & Ramanathan, V. Observational determination of albedo decrease caused by vanishing Arctic sea ice. *Proceedings of the National Academy of Sciences*, 111(9), 3322-3326. 2014.

Cao, Y., Liang, S., Chen, X., & He, T. Assessment of Sea Ice Albedo Radiative Forcing and Feedback over the Northern Hemisphere from 1982 to 2009 Using Satellite and Reanalysis Data. *Journal of Climate*, 28(3), 1248-1259. 2015.

The Pentland Centre for Sustainability in Business
Lancaster University
Lancaster
United Kingdom
LA1 4YX

T   +44 1524 510694
E   pentlandcentre@lancaster.ac.uk
W   www.lancaster.ac.uk/pentland
      @PentlandCentre

Connecting great minds in science to great minds in business